Evaluation of 3-D J-Integral in Cracked Pipe

By

Amit K. Pawar

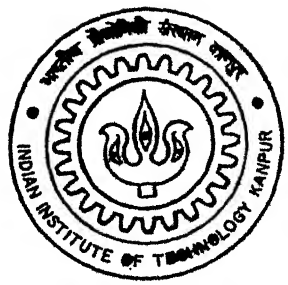

DEPARTMENT OF NUCLEAR ENGINEERING & TECHNOLOGY

INDIAN INSTITUTE OF TECHNOLOGY KANPUR

OCTOBER 2003

Evaluation of 3-D *J*-Integral in Cracked Pipe

A Thesis Submitted
in Partial Fulfillment of the Requirements
for the Degree of
Master of Technology

by

AMIT K. PAWAR

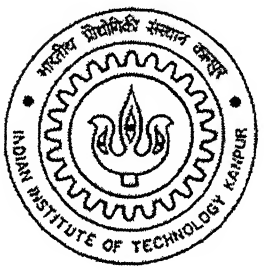

to the

DEPARTMENT OF NUCLEAR ENGINEERING & TECHNOLOGY

INDIAN INSTITUTE OF TECHNOLOGY KANPUR

OCTOBER 2003

CERTIFICATE

It is certified that the work contained in the thesis entitled "***Evaluation of 3-D J-Integra in Cracked Pipe***", by **Amit K.Pawar** has been carried out under our supervision and tha this work has not been submitted elsewhere for a degree.

Dr. Sumit Basu
Asst. Professor
Department of Mechanical Engg.
Indian Institute of Technology Kanpur

Dr. P. M. Dixit
Professor
Department of Mechanical Engg.
Indian Institute of Technology Kanpur

October, 2003.

Abstract

In the present work mathematical formulation of *J*-integral and its finite element implementation is presented. A Matlab code is developed for evaluating *J*-integral for two dimensional crack problems and is extended to determine three dimensional point-wise *J*-integral along a curved shape crack front. The results from the code are verified against standard elastic problems for which the analytical results are known.

Though the analysis of the components in nuclear industry involves geometric as well as material nonlinearity and the domain of *J*-integral is the elasto-plastic analysis, but as starting phase of the development of code, the *J*-integral is evaluated and validated in the context of Linear Elastic Fracture Mechanics (LEFM).

A parametric study is carried out for a pipe having circumferential semi-elliptical surface crack for different aspect ratios in the elastic region.

Acknowledgement

I wish to place on records my deep sense of gratitude and indebtedness to my supervisors Dr. P. M. Dixit and Dr. Sumit Basu for their expert guidance, valuable suggestions, personal encouragement and generous help during the course of my thesis work. They have introduced me to the exciting field of Fracture Mechanics. I am also thankful to Dr. B. K. Dutta for his expert guidance and personal encouragement and valuable suggestions.

I am thankful to my colleagues Sachin, Jaydeep, Santosh, Rajiv, Abhijit, sudhish, and Mr. R.K. Saxena of Finite Element Analysis Lab for their constant help and encouragement. I have so many unforgettable memories with them which I'll cherish forever.

I would like to thank all my friends for always being with me and bearing me through thick and thin. Special thanks are due to Vivek, Manas, Vinay, Amar, Rajit, Sudesh, Rajneesh, Saurabh, Rajat, Pradeep and others who made my life so beautiful here.

Amit Pawar

CONTENTS

List of Figures

LIST OF TABLES

CHAPTER 1
INTRODUCTION

1.1 GENERAL INTRODUCTION

Per capita power consumption is a measure of living standard in today's world. The major sources of power generation are fossil fuel, hydro power and nuclear power. While the reserves of fossil fuel are limited, the resources of the hydro power are highly dependent on the geographical topology, further, they are also limited. The share of nuclear energy is growing in power sector. In fact, it will be a major constituent of the energy sources in future.

The safety is of utmost concern in design and manufacturing of components of nuclear power plant. But at the same time the cost of power generation must be affordable. Loss of coolant accident (LOCA) is most likely to occur in the pressurized water reactor (PWR) plant. The scenario referred to as "thermal shock" involves the possibility of fracture of a nuclear reactor pressure vessel during a loss of coolant accident (LOCA).

One of the most likely causes of a loss of coolant accident in a nuclear power plant is a rupture in the piping system caused by stress corrosion. Many incidents of stress corrosion cracking have been reported. Consequently there is a great need for a quantitative understanding of the behavior of cracked pipe under normal operating and accident conditions — for example a seismic event. In most instances, the concern is for surface cracks that initiate at the inner surface of the pipe in the heat affected zone around a girth weld. Affected by the weld induced residual stress, these cracks tend to grow circumferentially and radially, sometimes attaining a size that is a significant fraction of pipe wall area. Fig. 1.1 shows an example of the cracks that were discovered in the wall

of 4-in diameter stainless steel pipes in the boiling water reactor (BWR) in 1974. This example shows that substantial crack sizes can be achieved before detection.

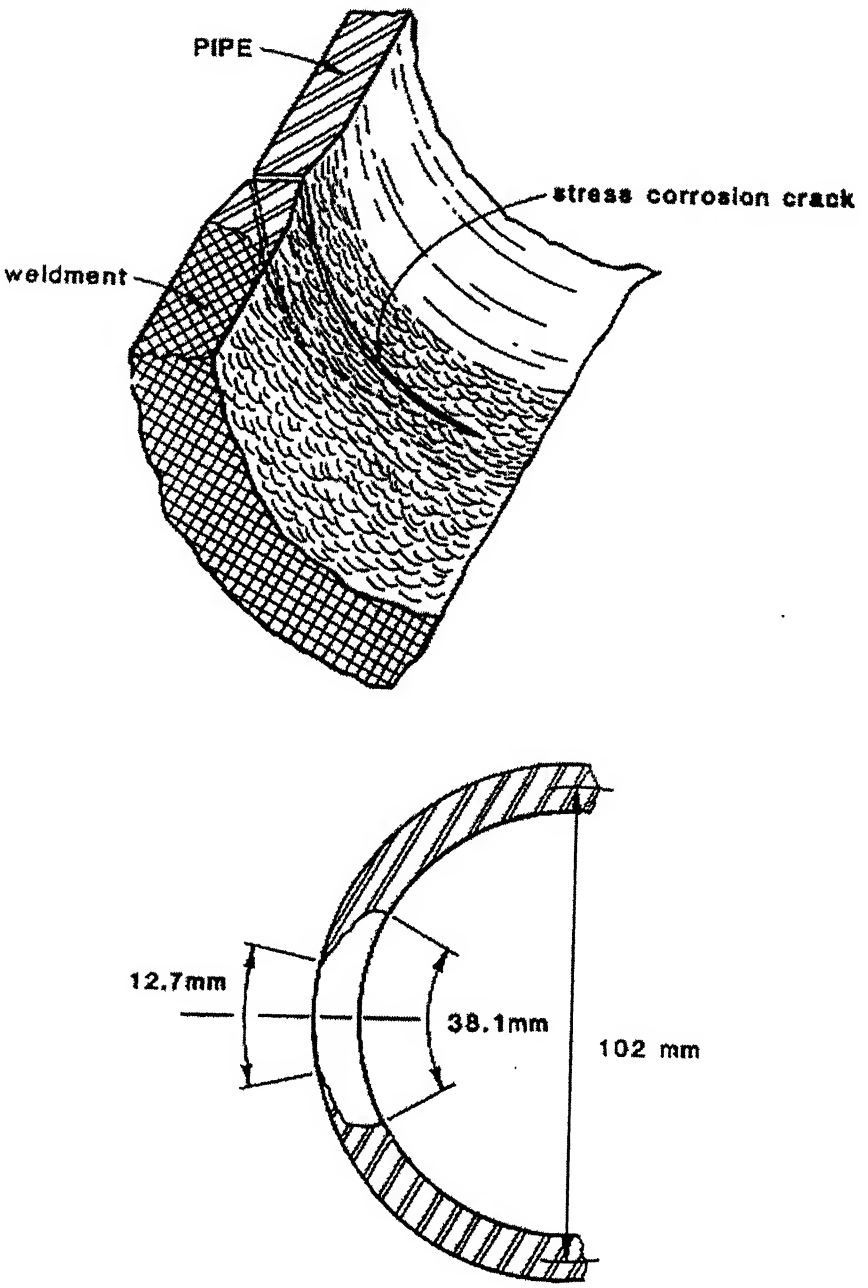

Figure 1.1Crack detected in 4-in diameter recirculation by-pass of a boiling water reactor plant

A prime consideration in analyzing cracked nuclear power plant pipes is to determine, if failure actually occurs, whether it will lead to a "leak-before-break-

condition". In general the leak-before-break concept refers to a pressure containment system failure event in which a part-through-wall crack extends to become a through wall crack, thus allowing contained fluid to escape. If no further crack growth occurs, then the loss of fluid can presumably be detected in one way or another and the system can be shutdown safely. The alternative – the through-wall crack propagates along the wall – will lead to a catastrophic event. Obviously it must be avoided. If failure occurs, it is very desirable to assure that it will be confined to the leak-before-break mode.

In nuclear power plant applications, it is necessary to show that the leak-before-break concept is the applicable failure mode in piping systems, where cracking has occurred or even could occur. Specially, it must be established that a pipe crack will be revealed by leak detection techniques before it reaches a condition where fracture could occur under normal operating or postulated accident condition. The design basis for accident used in nuclear plant regulation around the world is the so called full guillotine offset break (i.e., instantaneous circumferential fracture). This extreme condition has resulted in the incorporation of massive pipe whip restraints into nuclear piping systems. These restraints are not only very expensive to design and install, but they can reduce the reliability of in-service inspection while increasing the radiation hazard in the inspection process. The necessity of such devices in design stage and as modification in operating plants would be substantially relieved if leak-before-break conditions could be demonstrated. Consequently, there is currently a great deal of research interest in developing more precise fracture mechanics analysis methods.

The material of nuclear reactor pressure vessel is low alloy steel while the material of piping is stainless steel. It is difficult to join the two different materials because of their different crystalline structure. For joining the feritic steel and austenitic steel a thin layer of a different material, which is weldable to both the materials, known as buttering material is applied to one of the materials and then welding is done. This joint is obviously having lesser strength than a joint between the same materials. The joint between two materials having different crystalline structure is known as bimetallic joint. So this bimetallic joint between the pressure vessel and the piping is more vulnerable than other joints in the remaining piping.

1.2 REVIEW OF LITERATURE

The nuclear plant piping materials are very ductile and tough. In the materials selected for such service, crack growth is generally preceded by substantial crack-tip blunting while significant amount of stable crack growth can occur prior to the fracture instability. Linear elastic fracture mechanics techniques usually provide a very conservative prediction in such circumstances, conservatism that often prompts unnecessary remedial action. So J-integral is used to characterize the crack in the bimetallic welded pipe joint

J-integral is the most used crack tip integral in fracture mechanics. Its role in nonlinear fracture mechanics was introduced by Rice [1, 2] in 1968, who provided the interpretation of *J* as a measure of the intensity of deformation at notch or crack tip and, in the context of inelasticity, as energy release rate. Within the thermodynamics framework, the integral was introduced by Cherepanov [3] in 1967 as an extension of Griffith's approach to inelastic solids. Subsequently, the connection between *J* and Eshelby's energy momentum tensor was noted [4, 5]. Translational and nontranslational conservation integrals have been presented by Knowles and Sternberg [6]; the energetic force interpretations were made by Budiansky and Rice [7]. In this context *J*-integral is member of translational conservation integrals. However *J*-integral possesses additional features which make it unique among the conservation integrals. The integral is divergence free for a material which admits (nonlinear) strain energy function. Furthermore *J*-integral has the same value for all open paths beginning on one face of the crack and ending on the opposite face (this assumes that there are no contribution to the integral from the crack faces, a condition which is usually met in most crack problems). This special path independent property under fairly general conditions has been advantageously exploited in the development of nonlinear fracture mechanics. For example, the above noted path independence allows a direct computation of the strength of crack tip singularities by evaluating the line integral in regions remote from the crack tip or along the remote boundaries.

To the extent that the HRR singularity field (Hutchinson [8], Rice and Rosengren [9]) prevails over a distance which is larger than the fracture process zone and the zone of

the finite strain, the crack tip field can be said to be characterized by the value of J-integral and the onset of crack growth can be correlated with a critical value of J. The J value referred to here is evaluated on contour placed within a region dominated by HHR singularity. It is in this context that J is referred to as a crack tip parameter. In other words, the concept of a crack tip parameter is not tied to the property of global path independence. Nevertheless path independence has far reaching consequences, e.g. the value of crack tip parameter can be determined from the remote field. Within the deformation plasticity theory, J also has an energy based definition which has been used to derive useful formulae for its determination directly from the load-displacement record of a cracked body. In other words, while global path independence and the energy based definition are not essential to the concept of J as parameter characterizing the crack tip field, these features play important roles in an engineering fracture mechanics methodologies.

The evaluation of crack tip contour integrals in numerical studies is a potential source of inaccuracy. To circumvent these numerical difficulties, Kishimoto, Aoki and Sakata [10-12] and Alturi, Nishioka, Brust and their coworkers [13-19] have restated crack tip integrals as path and area integrals. These so called path-independent integrals contain two terms: a path integral evaluated along a remote contour and an area integral evaluated within the area enclosed by remote contour. In three dimensional crack problems, these path and area integrals generalize to surface and volume integrals respectively.

Accurate pointwise values of J along 3-D crack front have been obtained by Shih, Moran and Nakamura [20] and Nakamura, Shih and Freund [21]. Li, Shih and Needleman [22] have interpreted the method as an application of principal of virtual work and made the connection to the virtual crack extension technique of Parks [23, 24] and Hellen [25]. Under more restrictive conditions, a similar domain form was obtained by deLorenzi [26].

A unified approach to the derivation of crack tip and associated finite domain integrals has been presented by Moran and Shih [27] using a general balance statement as the starting point.

One of the common methods used to evaluate the displacements and stresses appearing in the expression of *J*-integral is finite element method.

1.3 OBJECTIVE OF THE PRESENT WORK

The problem considered in the present work is given for study by the **Computational Mechanics Section** of the **Reactor Safety Division (RSD)** of **Bhabha Atomic Research Centre (B.A.R.C.),** Mumbai. The problem is concerned with the assessment of structural integrity of a typical, bimetallic welded pipe joint. The joint connects the to the pressure vessel of the reactor made of different material. So the accurate analysis of this joint is necessary. Numerical methods like FEM offers a viable and reliable solution technique to assess the severity of a crack developed in the welded pipe joints.

The present work can be subdivided into two main parts, as detailed below, along with a brief description of each part:

1. To develop an efficient Matlab code to evaluate the *J*-integral for three dimensional body having crack and validate it with known problems.
2. To carry out a parametric study of a pipe joint having elliptical crack for different crack lengths and aspect ratios.

1.4 STRUCTURE OF THESIS

Mathematical formulation of J integral and its finite element implementation is described in Chapter 2. Finite element analysis package PATRAN/NASTRAN is used to generate the input data for finite element implementation of *J*-integral. Results and verification of the two dimensional and three dimensional problems are detailed in Chapter 3. Chapter 4 deals with actual pipe problem. Results and discussion for the pipe problem are given in Chapter 4. Scope for future works has been discussed in Chapter 5.

CHAPTER 2
MATHEMATICAL FORMULATION

2.1 INTRODUCTION

The study of a physical phenomenon usually involves two major tasks: Mathematical modeling of the physical process resulting in algebraic, differential or integral equations and solution of the resulting equation.

While the derivation of the governing equations for most problems is not unduly difficult, their solution by exact methods of analysis is a difficult task. In such cases, approximate methods of analysis provide alternative means of finding solutions.

The Finite Element (FE) method is one of the most popular methods of numerical analysis, in which, a given domain is represented as a collection of simple sub-domains, called finite elements, so that, it is possible to systematically construct the approximation functions over each element, needed in a variational or weighted-residual approximation of the solution of a problem.

In this chapter, the mathematical formulation of crack tip integral, and FE formulations for a 3D static stress analysis have been presented. First we discuss the general derivation for crack tip integral. Subsequently 2D and 3D specialization will be presented.

2.2 MOMENTUM BALANCE – CRACKTIP INTEGRAL

2.2.1 General derivation of crack tip integral

A general treatment of crack tip integral based on a variational form of momentum (or incremental momentum) balance is presented in this section.

Attention is restricted to small strains and the strain displacement relation takes the usual form

$$\varepsilon_{ij} = \left(u_{i,j} + u_{j,i}\right)/2. \tag{2.1}$$

In the absence of body forces the equation of motion (or balance of linear moment) is written as

$$\sigma_{ji,j} = \rho \ddot{u}_i, \tag{2.2}$$

where ρ is the mass density, $\sigma_{ij} = \sigma_{ji}$ is Cauchy stress and a superposed dot denotes the material time derivative. Taking the inner product of (2.2) with the velocity field, $\dot{u}_i$, and rearranging the resulting expression gives

$$\begin{aligned} \left(\sigma_{ji}\,\dot{u}_i\right)_{,j} &= \sigma_{ji,j}\,\dot{u}_i + \sigma_{ji}\,\dot{u}_{i,j} \\ &= \rho \ddot{u}_i\,\dot{u}_i + \sigma_{ji}\,\dot{u}_{i,j} \\ &= \dot{T} + \dot{W}, \end{aligned} \tag{2.3}$$

where the stress work density, W, and kinetic energy density, T, at the material particle are given by

$$\begin{aligned} W &= \int_0 \sigma_{ij}\dot{\varepsilon}_{ij}\,dt \;\Rightarrow \dot{W} = \sigma_{ij}\,\dot{\varepsilon}_{ij} = \sigma_{ij}\,u_{i,j} \quad \& \\ T &= \int_0 \rho \ddot{u}_i \dot{u}_i\,dt. \;\Rightarrow \dot{T} = \rho \ddot{u}_i \dot{u}_i. \end{aligned} \tag{2.4}$$

Equation (2.3) is a differential form of mechanical energy balance and is valid for any mechanical response.

The following fluxes are introduced for purpose of subsequent development

$$\varphi_j = \sigma_{ij}\,\dot{u}_i, \qquad \dot{\psi} = \left(\dot{W} + \dot{T}\right). \tag{2.5}$$

Here φ_j is identified as the mechanical work flux vector and $\dot{\psi}$ is the time rate of change mechanical energy density. The balance law (2.3) can be therefore written as

$$\varphi_{j,j} = \dot{\psi}. \tag{2.6}$$

The equation (2.6) is called general balance equation. Consider a small arbitrary volume V and a surface ∂V which surrounds the volume V. Integrating this expression over V and applying divergence theorem to the term on the left hand side yields

$$\int_{\partial V} \varphi_j m_j \, dS = \int_V \dot{\psi} \, dV, \tag{2.7}$$

where m_j is the outward unit normal to the surface ∂V. Here it is assumed that the fields are sufficiently smooth so that the divergence theorem may be applied. By applying divergence theorem to (2.3) the order of differential equation is reduced by one so the expression (2.7) can be viewed as a weak or variational form of linear moment balance. Since the variation field is velocity the expression (2.7) is also an integral form of mechanical energy balance.

Let v_i be the instantaneous velocity of the surface ∂V. Using the Reynolds Transport theorem on the right hand side of (2.7) yields

$$\int_{\partial V} \varphi_j m_j dS = \frac{d}{dt} \int_V \psi \, dV - \int_{\partial V} \psi \, v_j m_j \, dS. \tag{2.8}$$

The result (2.8) is simply a representation of mechanical energy balance for the volume V. This result is now specialized to the crack propagation and for the purpose of clarity attention is focused on planer crack problems.

Consider a two dimensional body with an extending crack oriented along the x_1 axis of a rectangular Cartesian coordinate system. The cracked body lies in the x_1 - x_2 plane with the crack plane given by $x_2 = 0$. The crack extends in its own plane along the x_1 axis with speed v. Define a vanishingly small crack tip region with a small contour Γ, which is fixed in the size and orientation with respect to the crack tip and is translating with crack tip at the speed v. As depicted in figure (2.1) the area bounded by the fixed material curve C_0 and the curve Γ is denoted by $A(t)$ and is free of singularities.

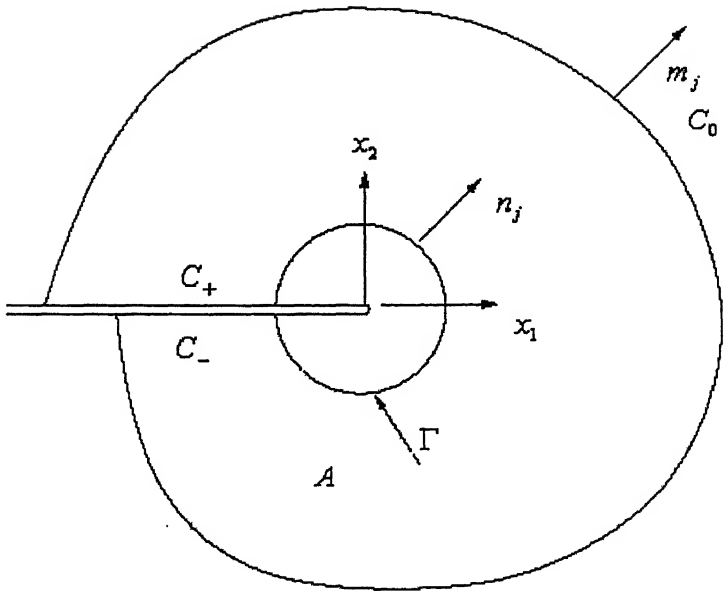

Figure 2.1 Conventions at crack tip. Domain A is enclosed by Γ, C_+, C_-, and C_0 .unit normal $m_j = n_j$ on C_+, C_- and C_0, and $m_j = -n_j$ on Γ.

Defining the contour $C = C_0 + C_+ + \Gamma + C_-$ which encloses $A(t)$. Without loss of generality, the crack faces are taken to be traction free. Rewriting the left hand side of expression in (2.8) for two dimensional case

$$\begin{aligned}\int_{\partial V} \varphi_j m_j \, dS &= \int_{C_0} \varphi_j m_j \, dS + \int_{C_+} \varphi_j m_j \, dS - \int_{\Gamma} \varphi_j n_j \, dS + \int_{C_-} \varphi_j m_j \, dS \\ &= \int_{C_0} \varphi_j m_j \, dS - \int_{C_+} \varphi_2 m_2 \, dS + \int_{\Gamma} \varphi_j m_j \, dS + \int_{C_-} \varphi_2 m_2 \, dS \\ &= \int_{C_0} \varphi_j m_j \, dS + \int_{\Gamma} \varphi_j m_j \, dS = \int_{C_0} \varphi_j m_j \, dC + \int_{\Gamma} \varphi_j m_j \, d\Gamma \, .\end{aligned}$$

Rewriting right hand side of the expression in (2.8) for two dimensional case

$$\frac{d}{dt}\int_V \psi\, dV - \int_{\partial V} \psi v_j m_j\, dS = \frac{d}{dt}\int_A \psi\, dV - \int_C \psi v_j m_j\, dS$$

$$= \frac{d}{dt}\int_A \psi\, dV - \int_{C_0} \psi v_j m_j\, dS - \int_\Gamma \psi v_j m_j\, dS$$

$$= \frac{d}{dt}\int_A \psi\, dV - \int_\Gamma \psi v_j m_j\, dS$$

$$= \frac{d}{dt}\int_A \psi\, dA - \int_\Gamma \psi v_j m_j\, d\Gamma.$$

Substituting $v_j = v\delta_{ij}$ and combining the left and right hand side as derived as two dimensional case of the expression (2.8) we get

$$\int_{C_0} \varphi_j m_j\, dC = \frac{d}{dt}\int_A \psi\, dA - \int_\Gamma (\varphi_j + \psi v\delta_{1j}) m_j\, d\Gamma. \tag{2.9}$$

It is noted that the only non-vanishing velocity on the boundary of $A(t)$ of consequence in (2.9) is $v_1 = v$ on Γ. The term on the left hand side of (2.9) is the rate at which the energy is being input into the body, the first term on the right hand side is the rate of increase of internal (mechanical) energy and consequently the last term is the instantaneous rate at which energy is being lost from the body due to flux through Γ. This quantity is denoted by F and is written for $n_j = -m_j$ on F,

$$F(\Gamma) = \int_\Gamma (\varphi_j + \psi.v\delta_{1j}) n_j\, d\Gamma. \tag{2.10}$$

There are two contributions to this flux integral. The first term represents the flux across Γ due to the material outside of Γ working on the material inside it. If Γ were a material curve this would be only contribution. The second term represents the contribution due to the flux of the material across Γ. The quantity G is defined as the limiting value of $F(\Gamma)/v$ as the contour Γ is shrunk on to the crack tip, i.e. G is the energy released from the body per unit crack advance (per unit thickness). For this concept to have physical significance, the limiting value G must be independent of actual shape of Γ in the limit $\Gamma \to 0$. In other words, the value of G must be path

independent in the limit $\Gamma \to 0$ (i.e. in the crack tip region). We now consider the condition under which G is finite and path independent in the limiting sense described.

Consider the closed path formed by two crack tip contours Γ_1 and Γ_2 and the crack face segments which connects the ends of the two contours. Application of divergence theorem to the closed contour integral yields

$$\begin{aligned} F(\Gamma_2) - F(\Gamma_1) &= \int_{A_{12}} \left(\varphi_j + \psi v \delta_{1j}\right)_{,j} dA \\ &= \int_{A_{12}} \left(\varphi_{j,j} + \psi_{,j} v \delta_{1j}\right) dA \\ &= \int_{A_{12}} \left(\varphi_{j,j} + \psi_{,1} v\right) dA \end{aligned} \tag{2.11}$$

where A_{12} is the area enclosed by the closed contour. By using (2.6) in (2.11) we obtain

$$F(\Gamma_2) - F(\Gamma_1) = \int_{A_{12}} \left(\dot{\psi} + v\psi_{,1}\right) dA. \tag{2.12}$$

If the integrand in (2.12) is $o(1/r^2)$ where $r = \sqrt{x_1^{\,2} + x_2^{\,2}}$ then $F(\Gamma_2) - F(\Gamma_1) = 0$ as $\Gamma_1, \Gamma_2 \to 0$ and path independence of F in the crack tip region $\left(\Gamma \to 0^+\right)$ is established. It is noted that this condition is satisfied if any field quantity f satisfied the following relation.

$$\dot{f} + v f_{,1} = o\left(f_{,1}\right) \quad \text{as } r \to 0^+, \tag{2.13}$$

where r is the radial distance from the moving crack tip. The condition (2.13) can be interpreted as a condition for locally steady state behavior. In particular if, ψ satisfies (2.13) then ψ is of the order of $1/r$, we have

$$\dot{\psi} + v\psi_{,1} = o\left(1/r^2\right) \quad \text{as } r \to 0^+, \tag{2.14}$$

and the path independence in the crack tip region is assured, it follows that on choosing Γ to be circular contour, (2.10) yields a finite value of F if the integrand of (2.10) is of order $(1/r)$, i.e.

$$\left(\varphi_j + \psi v \delta_{1j}\right) \approx A_j(\theta)/r + o(1/r) \quad \text{as } r \to 0^+, \tag{2.15}$$

for some $A_j(\theta)$ condition (2.14) may also be viewed as an integrability condition.

For field variables, φ and ψ, satisfying a balance law of (2.6) and for which local steady state conditions (2.13) and (2.15) hold, the integral given by (2.10) is path independent within the local crack tip region. It is noted that $\left(\dot{f} + v f_{,1}\right)$ is the time derivative of f with respect to a coordinate system which translate with the propagating crack and zero for a steady state condition. Thus the right hand side of (2.14) vanishes identically under the steady state crack propagation conditions and (2.10) provide a globally path independent integral for this class of problem for any material response.

With the understanding that the limiting value of flux $F(\Gamma)$, denoted by F is independent of shape of contour Γ as it shrunk on to the crack tip. The relation for F is written as

$$F = \lim_{\Gamma \to 0} \int_{\Gamma} \left(\varphi_j + v \psi \delta_{1j}\right) n_j \, d\Gamma. \tag{2.16}$$

A general representation for energy release rate can be derived using the general flux tensor H_{kj}. With its x_1 component denoted by H_{1j}, the general representation of energy release rate can be written as

$$J = \frac{F}{v} = \lim_{\Gamma \to 0} \int_{\Gamma} \mathrm{H}_{1j} \, n_j \, d\Gamma. \tag{2.17}$$

It follows from (2.16) that H_{1j} is defined by asymptotic relation

$$\mathrm{H}_{1j} \approx \left(\varphi_j + v \psi \delta_{1j}\right)/v \quad \text{as} \quad r \to 0^+. \tag{2.18}$$

The above relation is not written as an equality since the local steady state condition (2.13) will necessarily be invoked in defining H_{1j}. Assuming that the flux field in H_{1j} are sufficiently smooth and noting (2.6) and the asymptotic conditions (2.14) and (2.18), the condition for J to be finite can be restated as

$$\mathrm{H}_{1j} \approx A_j(\theta)/r + o(1/r) \quad \text{and} \quad b_1 = \mathrm{H}_{1j,j} = o\left(1/r^2\right) \quad \text{as } r \to 0^+. \tag{2.19}$$

It is noted that with (2.6) as the starting point no additional physical principle has been invoked to obtain result embodied in (2.16) and (2.17).

2.2.2 Mechanical energy integral

When φ_j and $\dot{\psi}$ are identified by (2.5) the flux integral (2.16) has the explicit form

$$F = \lim_{\Gamma \to 0} \int_{\Gamma} \left[(W + T) v \delta_{1j} + \sigma_{ij} \dot{u}_{i,1} \right] n_j \, d\Gamma. \tag{2.21}$$

The above relation is well known integral expression for crack tip mechanical energy flux. To obtain the corresponding result for energy release per unit crack advance J commonly referred to as energy release rate, we make the substitution $\dot{u}_i \approx -v u_{i,1}$ (i.e. local steady state condition (2.13) has been applied to the velocity field) and rearrange (2.20) to get

$$J = \lim_{\Gamma \to 0} \int_{\Gamma} \left[(W + T) \delta_{1j} - \sigma_{ij} u_{i,1} \right] n_j d\Gamma, \tag{2.22}$$

by formulation (and necessity) the loop Γ translates with the moving crack tip. Under the transient conditions or general material response, the energy release rate is given by the crack tip limit in (2.21), although the shape of the contour as shrunk on to crack tip is arbitrary.

Comparing (2.21) with expression (2.17), the integrand may be written more compactly as x_1 component of general energy tensor,

$$\mathrm{H}_{1j} = (W + T)\delta_{1j} - \sigma_{ij} u_{i,1}, \tag{2.23a}$$

the general energy tensor can be given by

$$H_{ij} = (W + T)\delta_{ij} - \sigma_{ij} u_{i,j}, \tag{2.23b}$$

2.3 A DOMAIN INTEGRAL EXPRESSION FOR THE ENERGY RELEASE RATE

2.3.1 Two-dimensional specialization

Consider a two-dimensional body and direct attention to a line a line crack along the x_1 axis. For arbitrary crack tip motion (but restricted to crack advance along the x_1 axis) under the dynamic conditions the energy release per unit crack advance is given by equation (2.22)

$$J = \lim_{\Gamma \to 0} \int_{\Gamma} \left[(W + T)\delta_{1j} - \sigma_{ij} u_{i,1} \right] n_j \, dC,$$

where W and T are the stress work and kinetic energy densities respectively, σ_{ij} and u_i are the Cartesian components of the stress and displacement, n_i is the unit vector normal to Γ and dC is the arc length as depicted in figure (2.2).

In the context of linear elastic material response, the result (2.22) is proposed by Atkinson and Eshelby [28] and independently derived by Kostrov and Nikitin [29] and Freund [30]. As noted by Nakamura et al. [31], "the general result (2.22) underlies virtually all crack tip energy integrals that have been defined and applied in fracture mechanics in the sense that each may be derived from (2.22) by invoking the appropriate restriction on material response (through W) and on the crack tip motion". It is also noted (2.22) was obtained from purely mechanical consideration. With usual reinterpretation of the field quantities with reference to undeformed configuration, (2.22) also hold in the context of finite deformation.

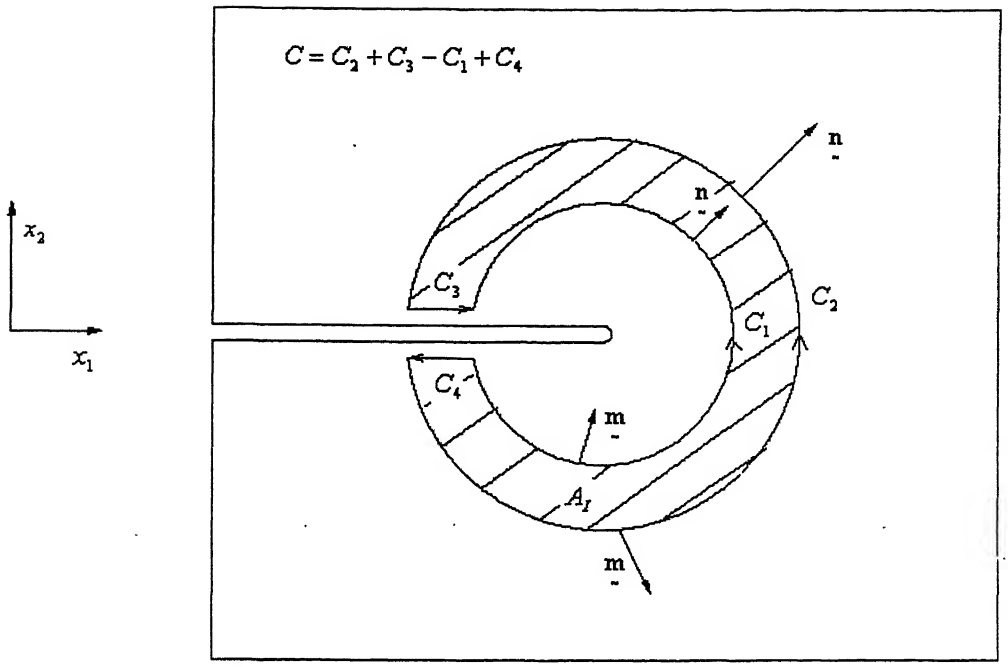

Figure 2.2 Simply connected region A_I enclosed by contour $C = C_2 + C_3 - C_1 + C_4$

Under quasi-static condition, $T = 0$, and (2.22) reduces to

$$J = \lim_{\Gamma \to 0} \int_{\Gamma} \left[W \delta_{1j} - \sigma_{ij} u_{i,1} \right] n_j \, dC. \tag{2.24}$$

For deformation theory solid, and in the absence of body forces, thermal strains and crack face traction the integral in (2.24) is path independent and its value does not depend on a limiting process in which the crack tip contour Γ shrunk onto the crack tip. The above result is due to Rice [1]. For this important case, the contour integral value for (2.24) can be accurately and readily extracted from the finite element field remote from the crack tip. It is noted that Eshelby introduced the conservation integral (2.24) in the context of a force on a dislocation or a point defect; under the isothermal conditions the bracketed quantity is x_1 component of energy momentum tensor H (see 2.23a).

The equation (2.24) can be rewritten as [20, 22]

$$J = \int_C \left[\sigma_{ij} u_{ij} - W\delta_{1i}\right] m_i q_1 \, dC - \int_{C_3+C_4} \sigma_{2j} u_{j,1} m_2 q_1 \, dC. \tag{2.25}$$

Here the closed curve $C = C_2 + C_3 - C_1 + C_4$, q_1 is the sufficiently smooth function in the region enclosed by C that is unity at C_1 and vanishes on C_2 and m_j is outward normal as depicted in Fig. 2.2; $m_1 = 0$, $m_2 = \pm 1$ on the crack faces, and $m_j = -n_j$ on C_1. The last term in (2.25) vanishes for traction free surfaces.

Within the framework of small deformation theory, the strain energy density can be written as the

$$W = \frac{1}{2}\sigma_{ij}\,\varepsilon_{ij} \tag{2.26}$$

Applying divergence theorem to closed contour integral in (2.25), we get

$$J = \int_{A_l} \left[\sigma_{ij} u_{j,1} - W\,\delta_{1i}\right]_{,i} dA - \int_{C_3+C_4} \sigma_{2j} u_{j,1}\, m_2\, q_1 \; dC \tag{2.27}$$

where A_l is the simply connected (area) domain enclosed by C. Now invoke the equilibrium condition and differentiating (2.26) with respect to x_1, we get

$$\sigma_{ij,j} + f_i = 0, \quad W_{,1} = \sigma_{ij}\,\varepsilon_{ij,1}, \tag{2.28}$$

to obtain the desired domain expression for the energy release rate

$$J = \int_{A_l} \left\{\left[\sigma_{ij} u_{j,1} - W\,\delta_{1i}\right] q_{1,i} - f_i\, u_{i,1} q_1\right\} dA - \int_{C_3+C_4} t_i\, u_{i,1}\, q_1\, dC. \tag{2.29}$$

Here f_i is the body force per unit volume and t_i is the traction on the crack faces. In the absence of body force and crack face traction, (2.29) reduces to

$$J = \int_{A_l} \left[\sigma_{ij} u_{j,1} - W\,\delta_{1i}\right] q_{1,i}\, dA, \tag{2.30}$$

which is energy release rate expression given in [22,26]. Equation (2.30) is domain independent in the sense that any annular (area) domain can be chosen for the purpose of

evaluating J. In this case the choice of domain is often dictated by convenience and mesh design. With the presence of thermal strain, body force and/or crack face traction, the domain integration for (2.30) must include the crack tip region $(r \to 0^+)$.

The function q_1 can be interpreted as imposing on the material points on C_1 a unit translation in x_1 direction while requiring the material points on C_2 to remain fixed. The material points within A_I are displaced according to any smooth interpolating function. In the context of a finite element model, C_1 is the arc formed by crack tip node/nodes. By letting C_1 coincide with the boundaries of different rings of the elements surrounding the crack tip, J can be evaluated on the alternate domains.

2.3.2 Three dimensional formulation

We consider a three dimensional crack front with a continuously turning tangent. Imagine that the plane shown in the Fig.2.2 is now the $x_1 - x_2$ plane of the local orthogonal Cartesian system depicted in Fig. 2.3a. Asymptotically, as $r \to 0^+$, plain strain condition prevail so that the three dimensional fields approach the (plain strain) two-dimensional fields at the crack front. Thus (2.24) defines the pointwise energy release rate which can be denoted by $J(s)$

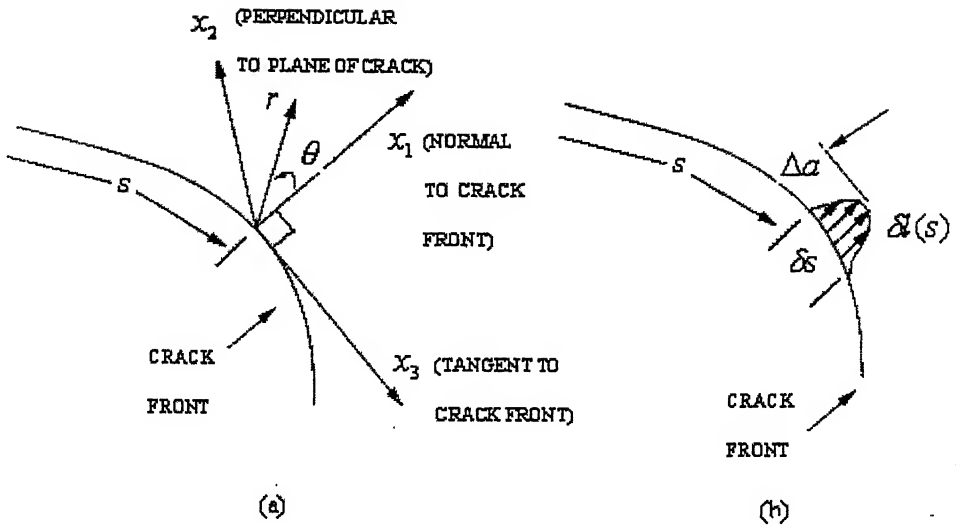

Figure 2.3 (a) Definition of the local orthogonal Cartesian coordinates at the point s on the crack front; the crack plane is in the $x_1 - x_3$ plane. (b) The function $\delta l(s)$ can be pictured as a virtual crack advance in the direction normal to the crack front in the crack front.

Let $\delta l(s)$ denote the local crack front advance at the point s in the direction normal to the crack front and in the plane of the crack, and let ds denote the elemental arc length along the crack front as depicted in the Fig.2.3(b). Recalling the definition *J*-integral, which states that it is the energy release rate per unit crack length advance i.e. $J = -d\Pi/da$ where $-d\Pi$ is decrease in potential energy at a point on crack front. Then to within first order in δl

$$-\delta\Pi = \bar{J}\Delta a = \int_{L_c} J(s)\delta l(s)\, ds. \tag{2.31}$$

where L_C denotes the line segment of crack front under consideration and δl is an arbitrary crack front advance. Here $-\delta\Pi$ is the decrease in potential energy and $\bar{J}$ is the energy released per unit of the finite segment of crack advance.

By separately advancing various segment of the crack front, the arc weighed pointwise $J(s)$ can be computed along a three dimensional crack front.

To fix ideas and minimize nonessential manipulations we focus our attention on a notch with notch thickness h as shown in Fig. 2.4 and argue (heuristically) that $h \to 0$ is

the sharp crack configuration of interest. The surface of the notch consists of faces S_A and S_B, with normals along x_2, and a face with a normal in the $x_1 - x_3$ plane. Now let the notch face S_t with normal m_k in the $x_1 - x_3$ plane, advances $\Delta a l_k$ in the x_k direction, i.e.

$$\Delta a . \underset{\sim}{\mathbf{l}} . \underset{\sim}{\mathbf{m}} = \delta l(s) \text{ or } \Delta a l_k m_k = \delta l(s) \tag{2.32}$$

Furthermore restrict l_k to be a function of x_1 and x_3 only; thus $l_2 \equiv 0$. Using (2.23b) and (2.32) in (2.31), we obtain

$$\bar{J} \Delta a = \Delta a \int_{S_t} \left[\sigma_{ij} u_{j,k} - W \delta_{ki}\right] l_k m_i \; ds. \tag{2.33}$$

When $\Delta a l_k$ corresponds to a translation, l_k can be taken outside of the integral sign and (2.33) gives $\bar{J} = l_k J_k$ where under isothermal conditions J_k are the translational conservation integrals (Budiansky and Rice [7]).

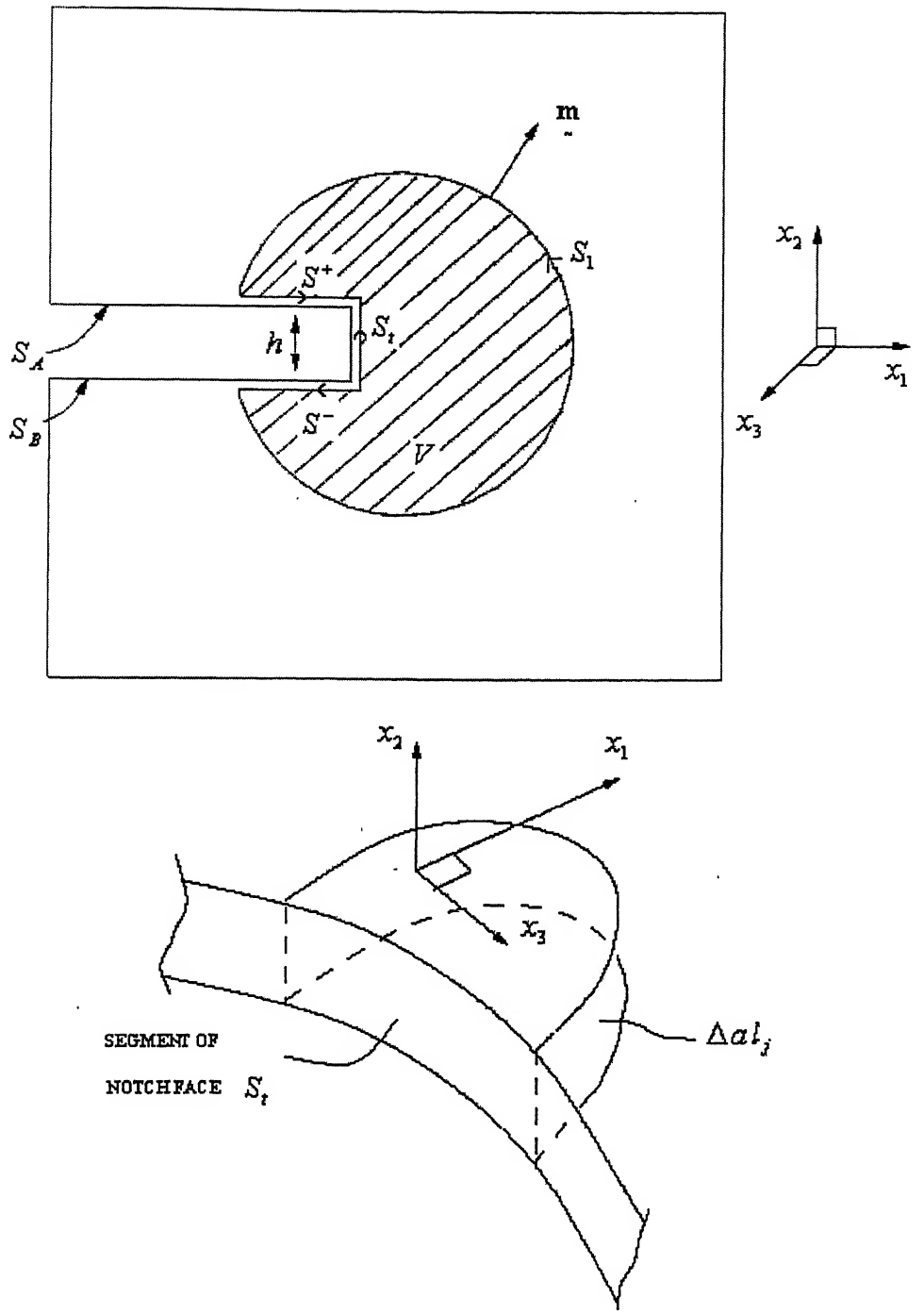

Figure 2.4(a) Schematic of body and volume V in the $x_1 - x_2$ plane containing a notch of thickness h ;note that $\mathbf{m} = -\mathbf{n}$ on S_t. (b) Schematic of notch face when the function $\Delta a l_k$ is interpreted as a virtual advance of a notch face segment in the direction normal to x_2

Consider the simply connected volume, V, enclosed by surfaces S_t, S^+, S^- and S_1 as depicted in Fig. 2.4(b). We introduce the function q_k defined by

$$q_k = \begin{cases} l_k & \text{on } S_t \\ 0 & \text{on } S_1 \end{cases} \tag{2.34}$$

together with the requirement that q_k be sufficiently smooth in the volume V. Using (2.34), (2.33) can be rewritten in the form of an integral over the closed surface S ($S = S_1 + S^+ + S^- - S_t$) plus the crack face terms,

$$\bar{J} = \int_S \left[\sigma_{ij} u_{j,k} - W \delta_{ki}\right] m_i \, q_k \, ds - \int_{S^+ + S^-} \sigma_{2j} u_{j,k} \, m_2 \, q_k \, ds. \tag{2.35}$$

To arrive at (2.35), following results have been used $m_1 = 0$, $m_3 = 0$ ($m_2 = \pm 1$), on the crack faces; it may be noted that $l_2 = q_2 = 0$ everywhere.

Application of divergence theorem to the closed surface integral in (2.35), and use of (2.28) yields

$$\bar{J} = \int_V \left\{ \left[\sigma_{ij} u_{j,k} - W \delta_{ki}\right] q_{k,i} - f_i u_{i,k} \, q_k \right\} dV - \int_{S^+ + S^-} t_i u_{i,k} \, q_k \, ds. \tag{2.36}$$

Now let $h \to 0$ to obtain the desired to obtain desired expression for the energy decrease when a local segment of crack front advances by $\Delta a l_k$ in its plane. In the absence of body force and crack face traction (2.36) reduces to

$$\bar{J} = \int_V \left[\sigma_{ij} u_{j,k} - W \delta_{ki}\right] q_{k,j}. \tag{2.37}$$

The domain expressions (2.36-2.37) give the energy release by the body per unit crack advance over a finite segment of the crack front. To a first approximation the pointwise energy release rate $J(s)$ may be assumed to constant over the small length L_C of crack front and can be brought out of the integral sign in (2.31) to yield,

$$J(s) = \frac{\bar{J} \Delta a}{\Delta a \int_{L_C} l_k(s) m_k(s) \, ds}, \tag{2.38}$$

where the term in the denominator is the increase of crack area due to the virtual crack advance at point s on the crack front and in $\bar{J}$ is evaluated over the volume which contains the length L_C.

2.4 FINITE ELEMENT FORMAULATION FOR THE VOLUME INTEGRAL METHOD

2.4.1 Two-dimensional implementation

For isoparametric elements, the coordinates (x_1, x_2) in the physical space and the displacements (u_1, u_2) for 8 noded element are written as

$$x_i = \sum_{K=1}^{8} N_K X_{iK}, \qquad u_i = \sum_{K=1}^{8} N_K U_{iK}, \qquad i = 1, 2 \tag{2.39}$$

where N_K are the bilinear shape functions, X_{ik} are the nodal coordinates and U_{iK} are the nodal displacements [32].

Consistent with the isoparametric element formulation, q_1 can be interpolated within an element as

$$q_1 = \sum_{I=1}^{8} N_I Q_{1I} \tag{2.40}$$

where Q_{1I} are nodal values for the I^{th} node. From the definition of q_1, if the I^{th} node is on C_1, $Q_{1I} = 1$, whereas if the I^{th} node is on C_2, $Q_{1I} = 0$. In the area between C_1 and C_2, Q_{1I} can be taken to vary between 1 and 0. Using (2.39),(2.40) and the chain rule, the spatial gradient of q_1 within an element is given by

$$\frac{\partial q_1}{\partial x_j} = \sum_{I=1}^{4} \sum_{k=1}^{2} \frac{\partial u_j}{\partial \eta_k} \frac{\partial \eta}{\partial x_j} Q_{1I}, \tag{2.41}$$

where $\partial \eta / \partial x_j$ is the inverse Jacobian matrix of the transformation (2.39).

With 2×2 Gaussian integration, the discretized from the domain expression for the energy release rate (2.29) for plane strain and plane stress problem is

$$J = \sum_{\substack{\text{all} \\ \text{elements} \\ \text{in } A_1}} \sum_{p=1}^{8} \left\{ \left[\left(\sigma_{ij} \frac{\partial u_j}{\partial x_1} - W \delta_{1i} \right) \frac{\partial q_1}{\partial x_i} - f_i \frac{\partial u_i}{\partial x_1} q_1 \right] \det\left(\frac{\partial x_k}{\partial \eta_k} \right) \right\}_p w_p$$

$$- \sum_{\substack{\text{all edges} \\ \text{on} C_3 + C_4}} \left\{ t_i \frac{\partial u_i}{\partial x_1} q_1 \right\} w. \qquad (2.42)$$

Here the quantities within $\{\ \}_p$ are evaluated at the 4 Gauss points and w_p and w are the respective weights. The crack face traction contribution can be evaluated using the equivalent nodal forces and spatial gradients of the nodal displacements or using standard integration procedure for boundary pressures [32]. (Note that the integration is carried out only on element edges on C_3 and C_4 with non-zero traction).

2.4.2 Three dimensional implementation

Consider a segment of the crack front, e.g., as shown in Fig 2.4. The limit $h \to 0$ has been taken to obtain the crack line identified by L_C. In the subsequent discussion L_C will be taken as the line connecting the nodes $M-1$, M and $M+1$ as shown in Fig. 2.5, and identify the volume V with the collection of elements which contains the line L_C. Consistent with the isoparametric formulation q_i within an element can be interpolated as

$$q_i = \sum_{I=1}^{8} N_I Q_{iI} \qquad i = 1, 2, 3, \qquad (2.43)$$

where N_I are the trilinear shape function and Q_{iI} are the nodal values for the I^{th} node. From the definition of q_k (see (2.34)), $Q_{iI} = 0$ if the I^{th} node is on S_1. For nodes inside V, Q_{iI} is given by interpolating between the nodal values on L_C and S_1; furthermore Q_{2I} vanishes identically.

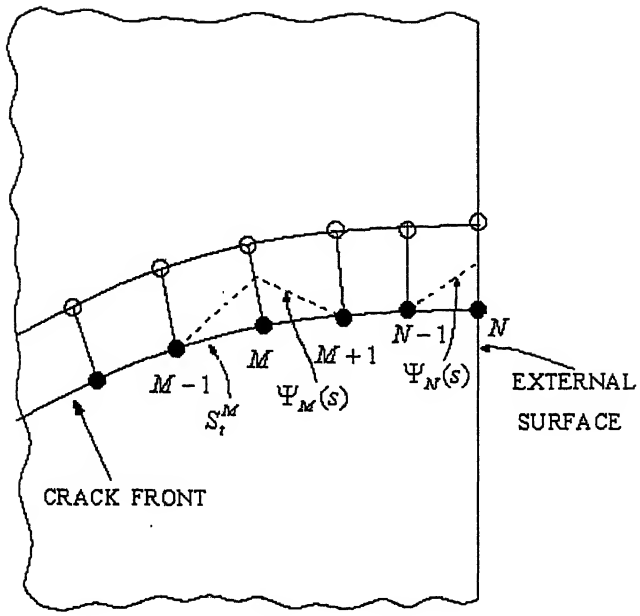

Figure 2.5 Schematic of the finite element mesh in the $x_1 - x_3$ plane illustrating the basis function for an "interior" node and "end" node along the crack front

Following the standard manipulations,

$$\frac{\partial q_i}{\partial x_j} = \sum_{I=1}^{8} \sum_{k=1}^{3} \frac{\partial u_j}{\partial \eta_k} \frac{\partial \eta}{\partial x_j} Q_{iI}, \tag{2.44}$$

where η_k are the coordinates in the isoparametric space. Employing $2 \times 2 \times 2$ Gaussian integration, the discretized form of the (2.36) is

$$\bar{J} = \sum_{\substack{\text{all} \\ \text{elements} \\ \text{in V}}} \sum_{p=1}^{8} \left\{ \left[\left(\sigma_{ij} \frac{\partial u_j}{\partial x_k} - W \delta_{ki} \right) \frac{\partial q_k}{\partial x_i} - f_i \frac{\partial u_i}{\partial x_k} q_k \right] \det\left(\frac{\partial x_k}{\partial \eta_k} \right) \right\}_p w_p$$

$$- \sum_{\substack{\text{all edges} \\ \text{on} C_3 + C_4}} \left\{ t_i \frac{\partial u_i}{\partial x_k} q_k \right\} w, \tag{2.45}$$

where $\bar{J}$ is the energy released for a unit virtual advance of a finite crack front segment. Here the quantities within $\{\ \}_p$ are evaluated at the 8 Gauss points and w_p and w are the respective weights. As discussed previously, the crack face traction contribution can

be evaluated using the equivalent nodal forces and the spatial gradients of the nodal displacements, or using the standard integration procedure for boundary pressure [32].

The relationship between $J(s)$ and $\bar{J}$ can be established by substituting (2.32) into (2.31) to get

$$\int_{L_c} J(s) l_j(s) m_j(s)\, ds = \bar{J}. \tag{2.46}$$

Now introduce piecewise continuous function for $J(s)$ and $l_j(s) m_j(s)$.

Let J_K denote the value of $J(s)$ at the K^{th} node on the crack front and $\Psi_k(s)$ be piecewise linear functions defined along the crack front. Then

$$J(s) = \sum_{K=1}^{N} J_K \Psi_K(s), \tag{2.47}$$

where N is the total number of nodes on the crack front and

$$\Psi_K = \begin{cases} 1 & \text{at the } K^{th} \text{ node} \\ 0 & \text{at all other nodes} \end{cases} \tag{2.48}$$

The nodal value J_K can be obtained using (2.38)

$$J_K = \frac{\bar{J}_K}{\int_{L_c} \Psi_K(s)\, ds}. \tag{2.49}$$

2.5FE FORMULATION FOR 3D STATIC ELASTIC STRESS ANALYSIS

Consider an arbitrary three-dimensional solid body Ω with volume V and boundary Γ as shown in Figure 2.6.

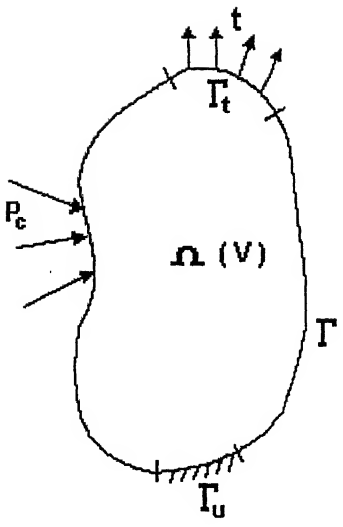

Figure 2.6 Domain and Boundary Conditions for Stress Analysis.

With reference to the Figure, Γ_u represents the boundary on which displacement is specified. Traction $\mathbf{t}$ is specified on the boundary Γ_t and $\mathbf{P_c}$ represents the concentrated forces acting on the body.

The principle of virtual work states that for a virtual perturbation in the displacement field at equilibrium, the virtual change in the internal strain energy (δU) must be balanced by an identical change in the external work (δW) due to the applied loads, that is:

$$\delta U = \delta W , \tag{2.50}$$

$$\text{or,} \quad \sum_e \delta U_e = \sum_e \delta W_e , \tag{2.51}$$

where, δU_e and δW_e are the contributions of the finite element e to the virtual change in strain energy and external work respectively.

Now,

$$\delta U_e = \int_{V_e} \{\delta\varepsilon\}^T \{\sigma\} dV_e , \tag{2.52}$$

where, V_e represents the volume of the element e,

$$\{\varepsilon\} = \text{Strain vector} = \begin{bmatrix} \varepsilon_{xx} & \varepsilon_{yy} & \varepsilon_{zz} & \varepsilon_{xy} & \varepsilon_{yz} & \varepsilon_{xz} \end{bmatrix}^T ,$$

$$\{\sigma\} = \text{Stress vector} = \begin{bmatrix} \sigma_{xx} & \sigma_{yy} & \sigma_{zz} & \sigma_{xy} & \sigma_{yz} & \sigma_{xz} \end{bmatrix}^T ,$$

Assuming an isotropic linear elastic material behaviour, (2.52) may be expanded as:

$$\delta U_e = \int_{V_e} \{\delta\varepsilon\}^T [D]\{\varepsilon\}\, dV_e , \tag{2.53}$$

where, $[D]$ is the material property matrix given by:

$$[D] = \frac{E}{(1+\upsilon)(1-2\upsilon)} \begin{bmatrix} 1-\upsilon & \upsilon & \upsilon & 0 & 0 & 0 \\ \upsilon & 1-\upsilon & \upsilon & 0 & 0 & 0 \\ \upsilon & \upsilon & 1-\upsilon & 0 & 0 & 0 \\ 0 & 0 & 0 & \frac{1-2\upsilon}{2} & 0 & 0 \\ 0 & 0 & 0 & 0 & \frac{1-2\upsilon}{2} & 0 \\ 0 & 0 & 0 & 0 & 0 & \frac{1-2\upsilon}{2} \end{bmatrix},$$

where, E is the Young's modulus of the material and υ is the Poisson's ratio;

The strains are related to the displacements as:

$$\{\varepsilon\} = \left[\frac{\partial u}{\partial x} \quad \frac{\partial v}{\partial y} \quad \frac{\partial w}{\partial z} \quad \left(\frac{\partial u}{\partial y} + \frac{\partial v}{\partial x}\right) \quad \left(\frac{\partial v}{\partial z} + \frac{\partial w}{\partial y}\right) \quad \left(\frac{\partial u}{\partial z} + \frac{\partial w}{\partial x}\right) \right]^T , \tag{2.54}$$

where, u, v and w represent the displacements of any arbitrary point within the element, in x, y and z directions respectively, and are interpolated from the nodal displacements through the element shape functions as:

$$\begin{Bmatrix} u \\ v \\ w \end{Bmatrix} = [N]\{u_e\}, \tag{2.55}$$

where, $[N]$ is the element shape function matrix and $\{u_e\}$ is the element nodal displacement vector.

From (2.54) and (2.55),

$$\{\varepsilon\} = [B]\{u_e\}, \tag{2.56}$$

where, $[B]$ is the strain-displacement matrix based on the derivatives of the element shape functions.

Combining (2.53) and (2.56) and noting that $\{u_e\}$ does not vary over the volume of the element:

$$\delta U_e = \{\delta u_e\}^T \int_{V_e} [B]^T [D][B] dV_e \{u_e\} \, dV_e . \tag{2.57}$$

Now,

$$\delta W_e = \{\delta u_e\}^T \int_{\Gamma_t^e} [N]^T \{t^e\} d\Gamma_t^e + \{\delta u_e\}^T \{P_c^e\}, \tag{2.58}$$

where, Γ_t^e is the area of the element that falls on Γ_t,

$\{t^e\}$ = Traction vector on $\Gamma_t^e = \begin{bmatrix} t_x^e & t_y^e & t_z^e \end{bmatrix}^T$,

$\{P_c^e\}$ = Concentrated nodal force vector.

Finally, substituting (2.57) and (2.58) into (2.51) and writing the Equation on element basis to give:

$$\sum_e \left\{ \delta u_e \int_{V_e} [B]^T [D][B] dV_e \{u_e\} \, dV_e \right\}^T = \sum_e \left(\{\delta u_e\}^T \int_{\Gamma_t} [N]^T \{t^e\} d\Gamma_t^e + \{\delta u_e\}^T \{P_c^e\} \right) \tag{2.59}$$

Now, since $\{\delta u_e\}^T$ is arbitrary, (2.59) reduces to:

$$\sum_e [K_e]\{u_e\} = \sum_e \{F_e^t\} + \sum_e \{P_c^e\} + \sum_e \{F_e^{th}\}, \tag{2.60}$$

where, $[K_e] = \int_{V_e} [B]^T [D][B] dV_e$ = Element stiffness matrix,

$\{F_e^t\} = \int_{\Gamma_t^e} [N]^T \{t^e\} d\Gamma_t^e$ = Element traction load vector,

$\{F_e^{th}\} = \int_{V_e} [B]^T [D]\{\varepsilon_{th}\} dV_e$ = Element thermal load vector.

The element matrices and load vectors of all the elements in the domain are assembled together to get the global stiffness matrix $[K]$ and the global load vector $\{F\}$ such that:

$$[K]\{u_g\} = \{F\},$$

where, $\{u_g\}$ is the global nodal displacement vector.

CHAPTER 3
VERIFICATION AND VALIDATION OF RESULTS

3.1 INTRODUCTION

The closed form solutions for the stress intensity factor (SIF in mode-I) of simple test specimens like Compact Tension (CT), Single Edge Notch Bend (SENB) specimen and Centre-Cracked-Plate (CP) are known. In elastic region, a relation between J and K_I exists. So the value of J can be evaluated accurately for a simple elastic problems. Thereby, the code can be verified with the help of these problems. First, the code for 2D case is verified for the SENB, CT and CP specimens under plane strain. Subsequently the code for 3D case is verified for solving the same set of problems with thickness is taken into consideration.

3.2 DESCRIPTION OF ANALYSIS

The stress analysis is performed using the PATRAN/NASTRAN FEM package. To determine the stresses at the Gauss points, first the nodal coordinate and displacement data is extracted from the analysis and then, with the help of these displacements, stress tensor, strain energy and finally J integral are evaluated using a Matlab code.

For 2-dimensional problems, 8-noded isoparametric quadratic elements have been used and the problems are analyzed in plain strain conditions. For three dimensional cases, 8-noded trilinear brick elements have been used.

3.3 VERIFICATION OF CODE FOR TWO DIMENSIONAL PROBLEMS

The results obtained from the Matlab code are verified for three different problems: SENB, CT and CP specimen. For two dimensional cases, the domain for *J*-integral is an area bounded by two curves around the crack as shown in Fig. 2.2. As discussed previously, in the absence of crack face traction and thermal strain, the inner boundary of the domain need not be too close to the crack tip. In this way, the stress field near the crack tip (which may contain some inaccuracies) does contribute to the calculation of J integral. In fact, the variation in J values for two dimensional cases is less then 0.1% for the domains well within the specimen (far from the specimen boundary).

3.3.1 SENB Specimen

Geometry of the specimen is shown in Fig. 3.1. The specimen is symmetric with respect to the plane in which the notch lies. We analyze only half of the specimen taking benefit of the symmetry. The mesh with boundary conditions is shown in Fig. 3.2 in which 1 represent constrain in X direction and 2 represent constraint in Y direction.

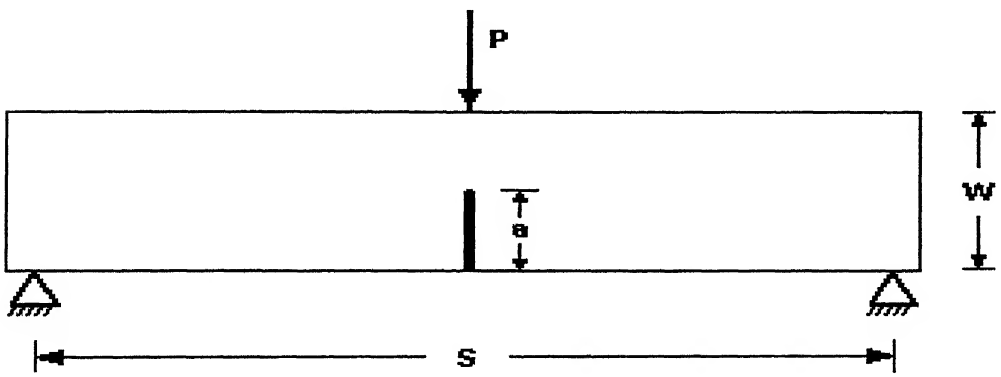

Figure. 3.1 SENB specimen (2D test problem).

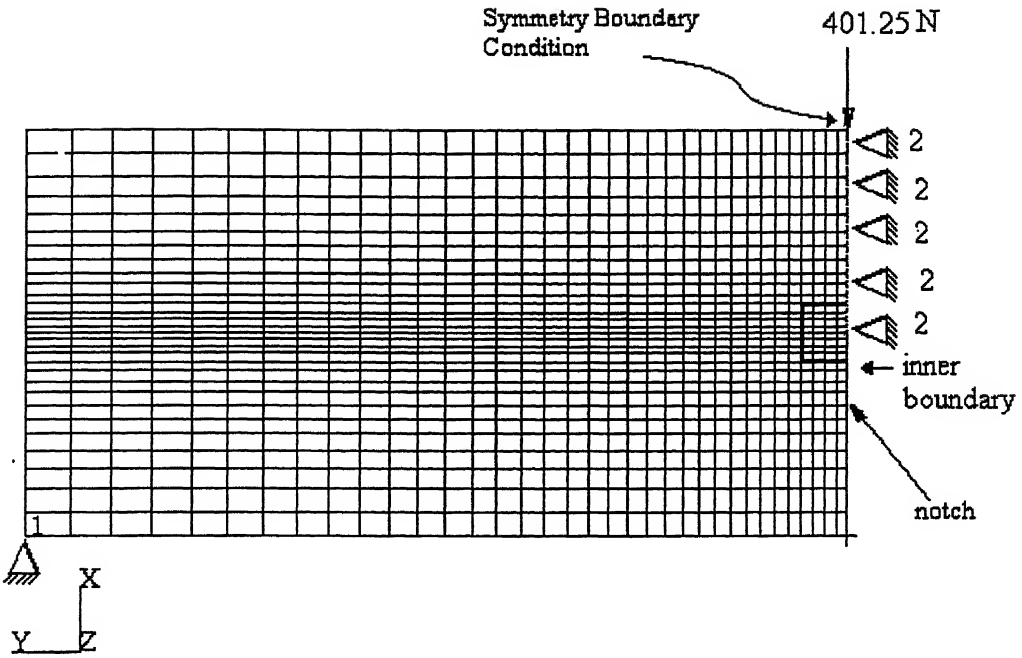

Figure. 3.2 Mesh (with B.C. and loading) for 2-dimensional SENB test specimen

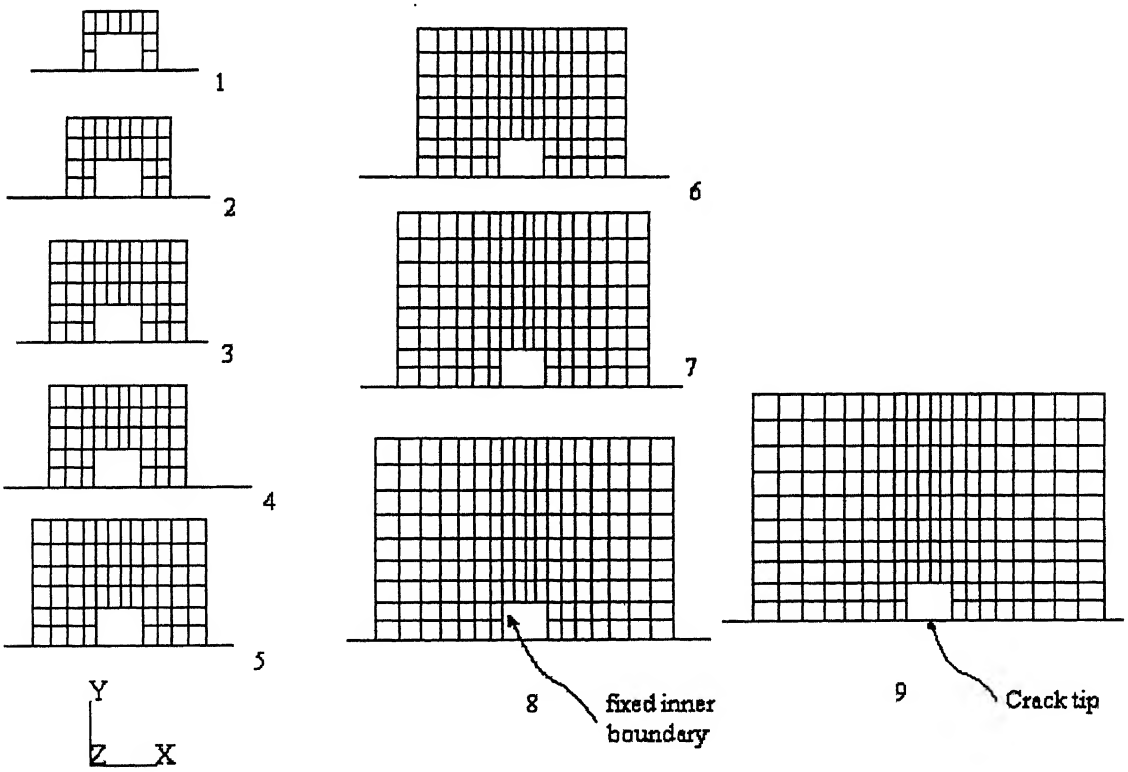

Figure 3.3 Domain selection.

The analytical expression for the Stress Intensity Factor K_I for the SENB specimen is given by [34]

$$K_I = \frac{PS}{BW^{3/2}} f(\alpha); \qquad \alpha = \frac{a}{W}, \tag{3.1}$$

where, B = Plate thickness

and $$f(\alpha) = \frac{3\alpha^{1/2}\left[1.99 - \alpha(1-\alpha)\left(2.15 - 3.93\alpha + 2.7\alpha^2\right)\right]}{2(1+2\alpha)(1-\alpha)^{3/2}} \tag{3.2}$$

In the elastic region the relationship between J-integral and K_I for the plane strain case can be written as

$$J = \frac{K_I^{\,2}}{E}\left(1-\upsilon^2\right), \tag{3.3}$$

where E and υ are elasticity constants.

The model dimensions and loading for analysis are taken from [33], and are the following.

Span $S = 4\ W = 101.6\ mm$
Width $W = 25.4\ mm$
Crack Length $a = 12.7\ mm$
Plate Thickness B = $25.4\,mm$ (3.4)
$a/W = 0.5$
Applied load $P = 802.5\,N$
Analysis load = $P/2 = 401.25$ N

To demonstrate the domain independence of J-integral, it is evaluated on a number of domains. A set of domain can be created as shown in Fig. 3.3. Domains are obtained by adding layer of elements to a smaller domain. Several contours are taken in each domain (see Table 3.1) by making the inner boundary layer (pushing it closer to the outer boundary). We evaluated the J-integral corresponding to each of these domains and results are tabulated in the Table 3.1. This table contains values of the J-integral for 9 sets of domains shown in Fig. 3.3. In the first set there are 14 contours and in the subsequent sets the number of contours decrease. This is because in each set the outer

boundary of the outermost domain (domain in 14th row) is fixed and the inner boundary is moving outwards so each time the number of domain is decreased by one.

Table 3.1 Values of J-integral (in N/m) for different sets of domains corresponding to different inner boundaries for a theoretical J-integral value of $18.40\ N/m$.

	1	2	3	4	5	6	7	8	9
1	18.7284								
2	18.7307	18.7318							
3	18.7334	18.7348	18.7372						
4	18.7347	18.7356	18.7370	18.7367					
5	18.7356	18.7363	18.7373	18.7373	18.7378				
6	18.7360	18.7364	18.7371	18.7371	18.7372	18.7367			
7	18.7362	18.7364	18.7369	18.7368	18.7368	18.7364	18.7361		
8	18.7364	18.7365	18.7369	18.7368	18.7368	18.7365	18.7364	18.7366	
9	18.7365	18.7365	18.7368	18.7368	18.7368	18.7365	18.7365	18.7366	18.7365
10	18.7365	18.7365	18.7368	18.7367	18.7367	18.7366	18.7365	18.7366	18.7372
11	18.7365	18.7365	18.7367	18.7367	18.7367	18.7366	18.7365	18.7366	18.7371
12	18.7365	18.7366	18.7368	18.7368	18.7368	18.7367	18.7367	18.7367	18.7375
13	18.7398	18.7399	18.7403	18.7405	18.7407	18.7409	18.7413	18.7419	18.7431
14	18.7845	18.7863	18.7886	18.7910	18.7941	18.7977	18.8025	18.8088	18.8173

From the table, it is clear that the difference in the values of the J-integral for different domains is very less (less than 0.1%) for the domains well within the specimen. This error can completely attributed to numerical rounding off during evaluation of integration and loss of accuracy in data transfer from PATRAN. As we move downward in the table, the outer boundaries of the domains get closer to the specimen. Some portion of the outer boundaries of the domains corresponding to 14th row coincides with the specimen boundaries where the stress values are not accurate and hence the deviation in J value in these cases from the mean value of $18.7364\ N/m$ is more.

From Equation (3.1), (3.2) and (3.3) we can evaluate the value of J-integral in the elastic region for SENB specimen with dimensions and loading given by (3.4). The value of J-integral is found to be$18.40\ N/m$. The same specimen has been analyzed by [34] and the value of J is found to be$18.46\ N/m$. The error in evaluating J-integral from the code is 1.82 % (with respect to J obtained from the formula).

3.3.2 CT Specimen

The geometry of the CT specimen is depicted in Fig. 3.4. The specimen is being symmetric with respect to the plane in which the notch lies. We analyze only half of the specimen using the symmetry. The mesh with boundary conditions is shown in Fig. 3.5.

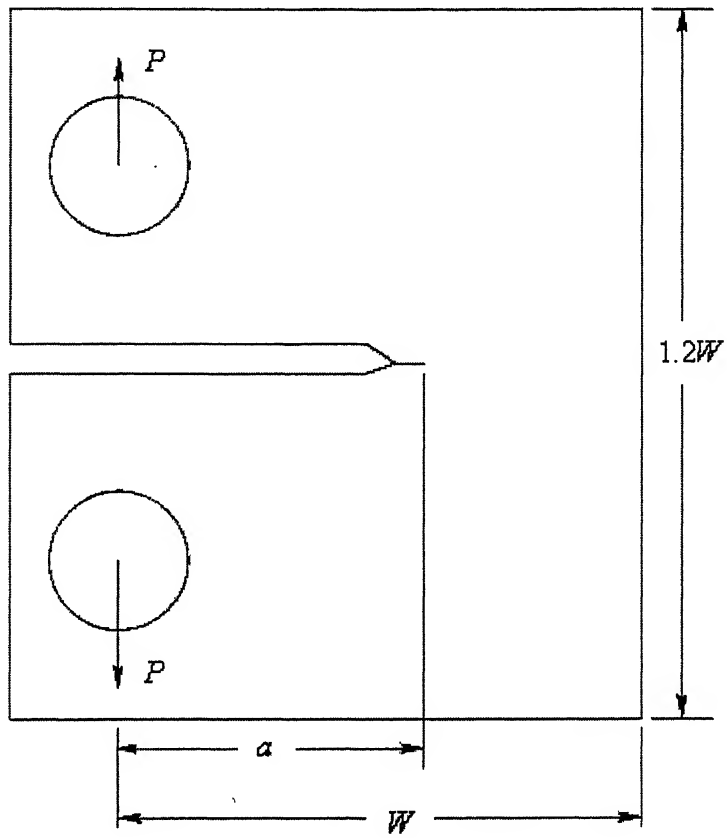

Figure 3.4 Compact tension (CT) specimen.

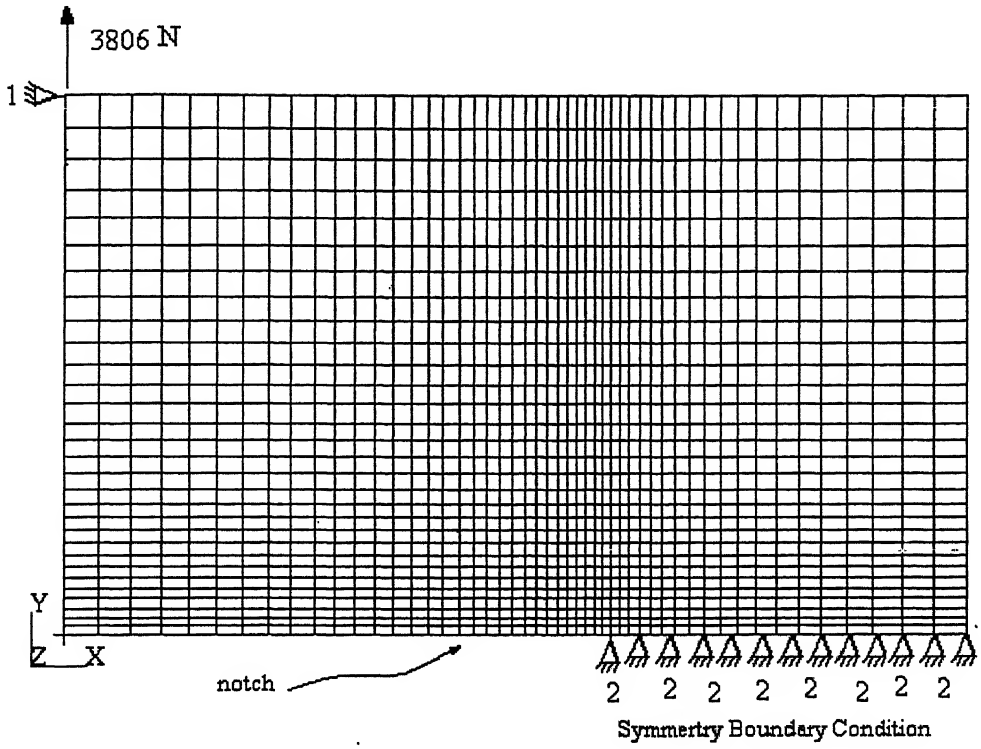

Figure 3.5 Mesh (with B.C. and loading) for CT specimen.

The analytical formula for Stress Intensity Factor K_I for CT specimen is given by [34]

$$K_I = \frac{P}{BW^{1/2}} f(\alpha); \qquad \alpha = \frac{a}{W}, \tag{3.5}$$

where, B = Plate thickness

$$f(\alpha) = \frac{(2+\alpha)\left(0.886 + 4.64\alpha - 13.32\alpha^2 + 14.72\alpha^3 - 5.6\alpha^4\right)}{(1-\alpha)^{3/2}}. \tag{3.6}$$

Here E and υ are elasticity constants.

The model dimensions and loading for analysis are taken from [33], and are:

$$\begin{aligned} &\text{Crack length } a = 14.9 \ mm \\ &\text{Width } W = 25 \ mm \\ &\text{Thikness B} = 25.2 \ mm \\ &a/W = 0.596 \\ &\text{Applied load } P = 3806 \ N. \end{aligned} \tag{3.7}$$

We evaluated J-integral on the same sets of domains and found the similar trend for this specimen too. The results for few domains are tabulated below.

Table 3.2 Values of J - integral evaluated on different domains for CT specimen.

Domain	J-integral (in N/m)
1	710.8870
2	710.9680
3	710.9682
4	710.9336
5	710.9434
6	710.9434
7	710.9494
8	710.8828

Value of J-integral as obtained using (3.5), (3.6) and (3.3) using the dimensions and loading given by (3.7) is $723.2\,N/m$. The error in evaluating J-integral from code is 1.7 %.

3.3.3 Centre-Cracked Plate under uniform tension

The geometry of the center-cracked plate is depicted in Fig 3.6 again, using the symmetry of the problem, we analyze only one fourth of the model. The mesh with boundary condition is shown in Fig.3.7 in which 1 represent constrain in X direction and 2 represent constraint in Y direction.

The analytical expression for Stress Intensity Factor K_I for CP specimen is given by [35]

$$K_I = \sigma\sqrt{\pi a}\; f(\alpha); \qquad \alpha = \frac{a}{W}, \tag{3.8}$$

and $$f(\alpha) = 1.0 + 0.128\,\alpha - 0.288\,\alpha^2 + 1.523\,\alpha^3 \tag{3.9}$$

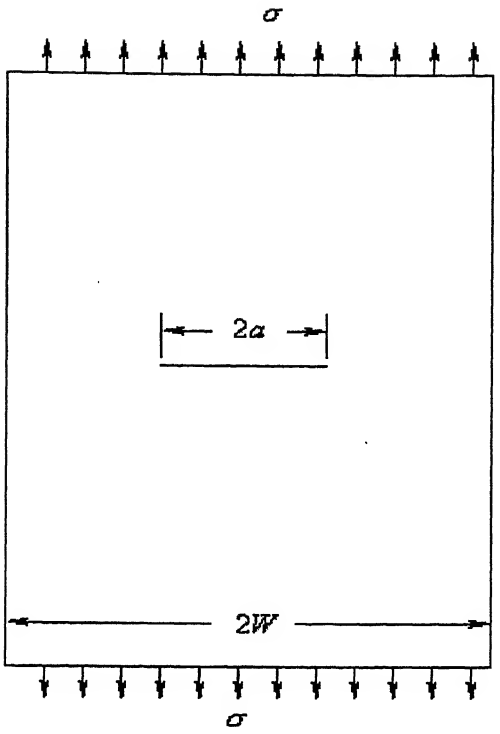

Figure 3.6 Centre-Cracked Plate under uniform tension

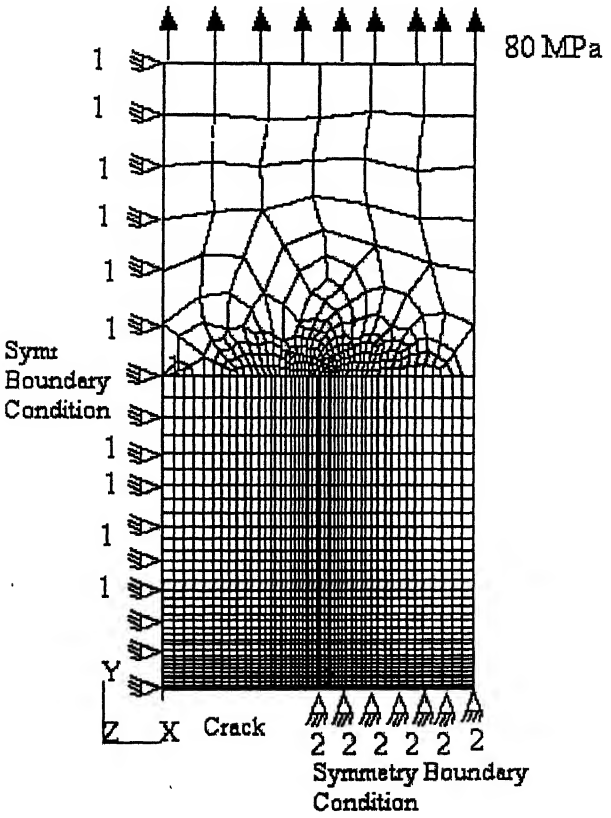

Figure 3.7 Mesh for Centre-Cracked Plate

The model dimensions and loading for analysis are as follows

$$\begin{aligned} &\text{Crack length } a = 0.25\ m \\ &\text{Width } W = 0.5\ m \\ &a/W = 0.5 \\ &\text{Applied traction } t = 80\,MPa \end{aligned} \tag{3.10}$$

We evaluated J-integral on the same sets of domains and again found the similar trend for this specimen too. The results for few domains are tabulated below.

Table 3.3 Values of J - integral evaluated on different domains for CP specimen.

Domain	J-integral (in N/m)
1	30633.0
2	30633.0
3	30632.6
4	30632.2
5	30632.6
6	30632.4
7	30632.6
8	30632.6

Value of J-integral as obtained using (3.8), (3.9) and (3.3) using the dimensions and loading given by (3.10) is 30451 N/m. The error in evaluating J-integral is 0.6 %.

3.4 VERIFICATION OF CODE FOR THREE DIMENSIONAL PROBLEMS

The 3-D Matlab code is used to obtain the *J*-integral values in the same specimen used in sec 3.3. For three dimensional case the domain is a volume bounded by the surfaces which surround the crack-front, such that the inner boundary of the domain coincides with the crack front. In this way the stress field near the crack front (which contains some inaccuracies) induces some error into the value of *J*-integral is not as accurate as obtained for 2D case. In fact, the variation in *J* values for first domain, which is nearest to the crack front (and consists of layer of single element around crack front), is highest. As the number of elements in the domain increases, the value of *J*-integral approaches to the theoretical value.

3.4.1 SENB Specimen

The geometry and the mesh are shown in Fig. 3.8(a) and 3.8(b) respectively. We have taken the same specimen and loading as in case two dimensional case (see sec. 3.2). If we consider the thickness of the specimen in z direction then specimen is symmetric with respect to the x-y plane. The specimen is also symmetric with respect to the plane in which the crack lies. Hence we analyze only one fourth of the specimen.

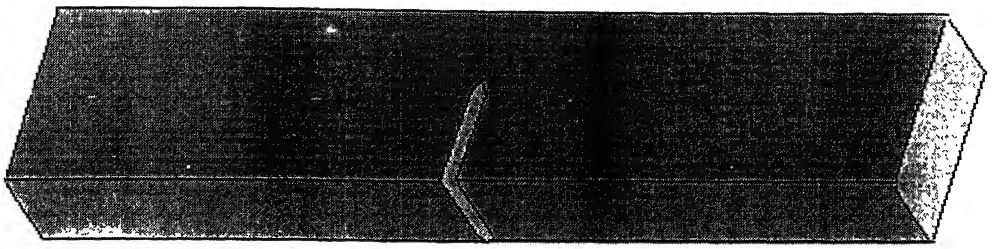

(a).

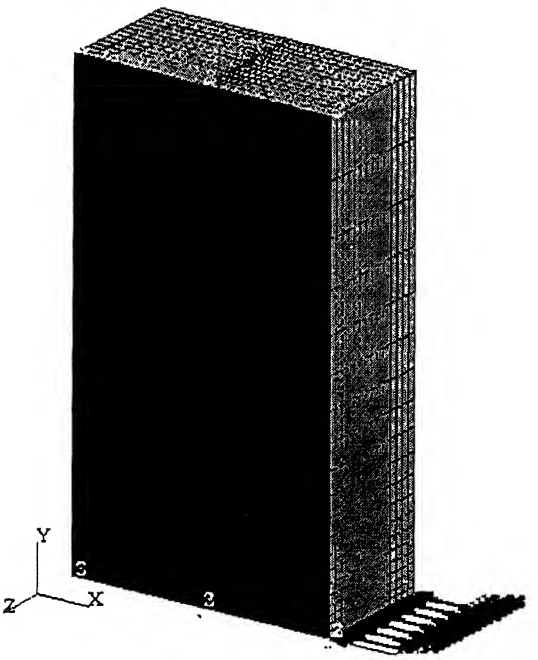

(b)

Figure 3.8 (a) 3-d SENB Specimen(b) Mesh For SENB Specimen.

Fig. 3.9 shows the variation of J-integral (in N/m) along the crack front. The pointwise J-integral is evaluated over 10 domains.

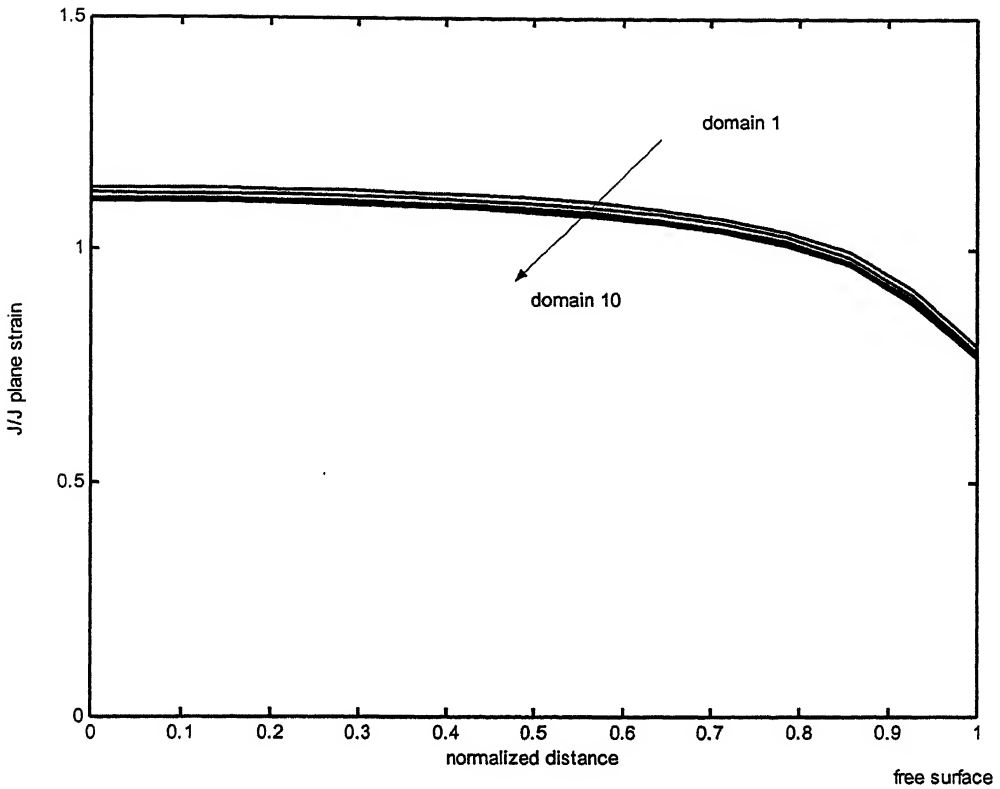

Figure 3.9 Variation of point-wise *J*-integral along the crack front for SENB specimen.

From the Fig. 3.9, it is clear that in the middle of the specimen, where there is plain strain condition prevails, the value of *J*-integral approaches a value slightly above (about 10%) that of plain strain case ($18.7\,N/m$). As we move towards the free surface the value of *J*-integral decreases. Similar trend has been obtained for SENB specimen by Shih et. al.[20]. For the first domain, the deviation of pointwise *J* value is largest in the plane strain region in the middle of the domain. As we increase the elements in the domain by adding more layers of elements, the pointwise *J*-integral value approaches to plain strain value in the middle of the domain. From the Fig. 3.9 it is also clear that the domain with only three layers of element is sufficient to get approximate value of *J*.

3.4.2 CT Specimen

We have taken the same specimen and loading as in two dimensional case. Again only one fourth of the specimen is analyzed on account of the symmetry Fig. 3.11 shows the

is evaluated over 10 domains. The mesh of CT specimen used in analysis is shown in Fig. 3.10.

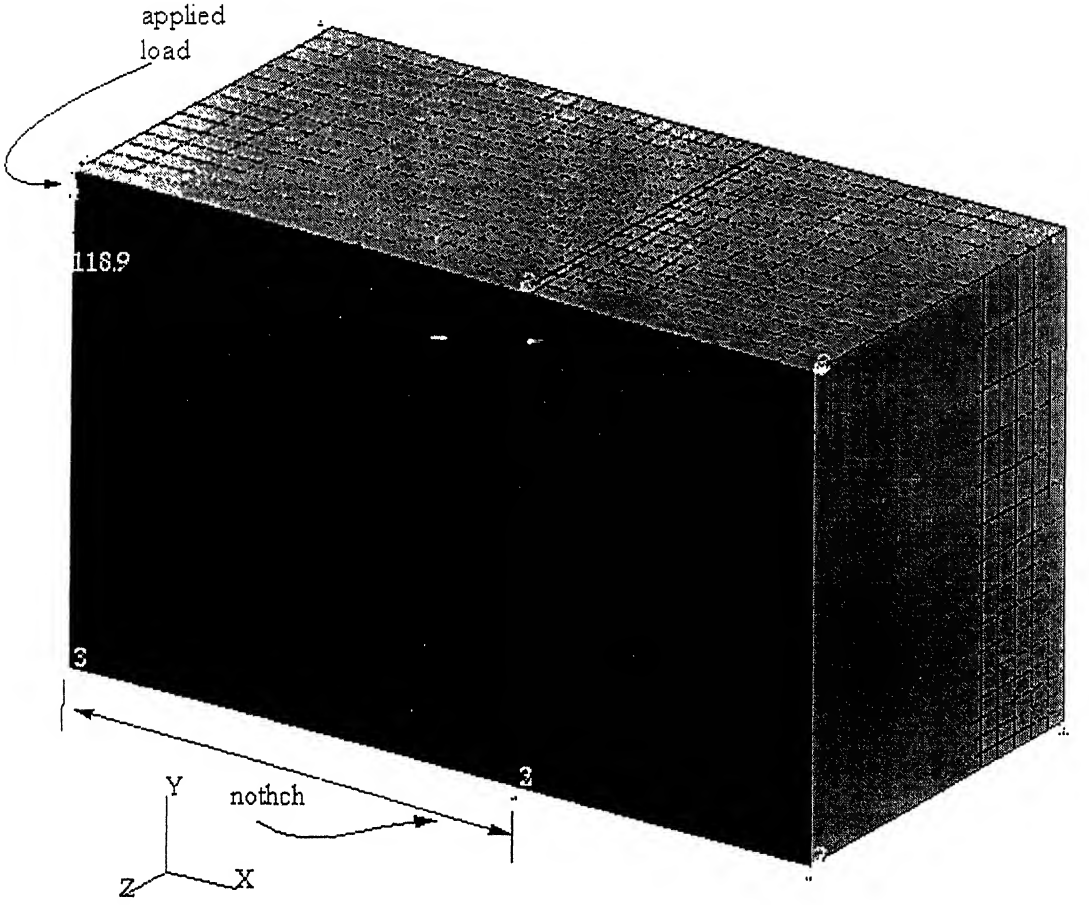

Figure 3.10 Mesh for 3-d CT specimen

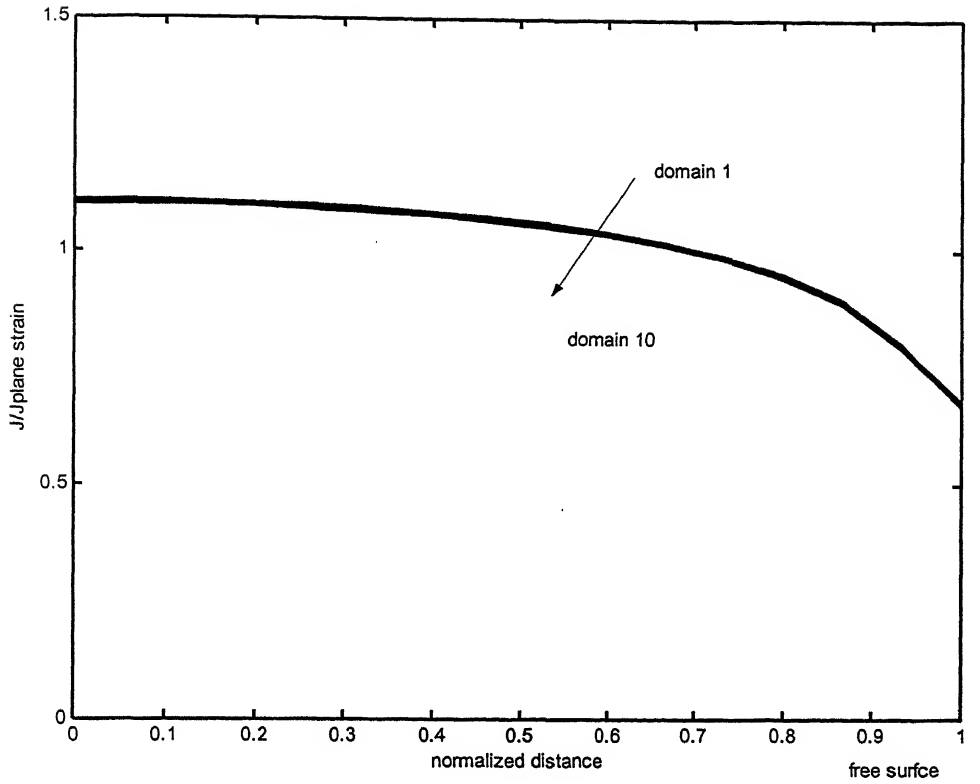

Figure 3.11 Variation of pointwise J-integral along the crack front for CT specimen

Similar trend as in case of SENB specimen is obtained here. In the middle of the specimen, the value of J close the plain strain of $710\,N/m$ and as we move toward the free surface the value of J-integral decreases. The value of J-integral again is slightly greater (about 10%) than the plane strain case ($710\,N/m$) in the middle of the specimen.

3.4.3 Centre-Cracked-Plate under uniform tension

Fig. 3.10 shows the variation of point-wise J-integral (in N/m) along the crack front. The point-wise J-integral is evaluated over 10 domains.

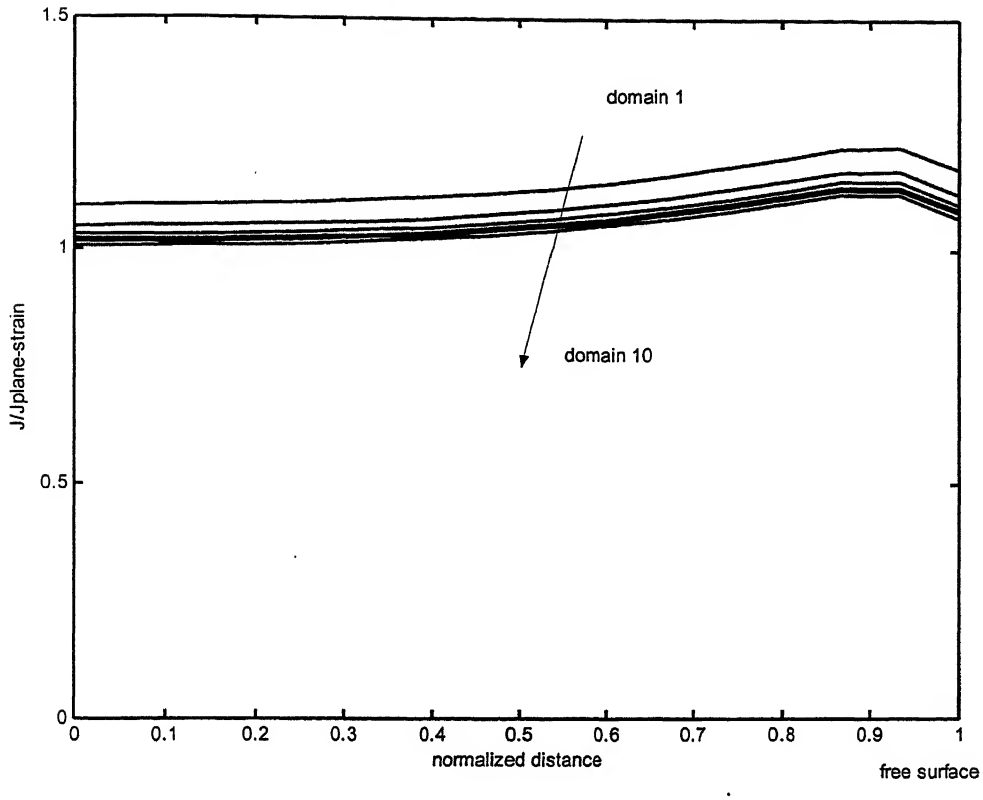

Figure 3.12 Variation of pointwise *J*-integral along the crack front for Centre-Cracked-Plate

The trend obtained for this case (Fig. 3.12) is slightly different than the trends which have been obtained previously. As we move in thickness direction from the middle thickness of the plate to free surface the value of point-wise *J*-integral increases and then decreases near the free surface. The value of *J*-integral approaches a value slightly (less than 5% for higher domains) above the plane strain value ($30630 N/m$) in the middle of the specimen.

CHAPTER 4
RESULTS AND DISCUSSIONS

4.1 INTRODUCTION

Welded joints are used to join a pipe to the nozzle of the pressure vessel. Because of the welded joint at the intersection, there always exists a possibility of an initial flaw. Due to the high stresses and corrosion, an existing flaw may grow into a surface crack. Though the actual shapes of such cracks are not simple, it has been observed that they are usually almost semi-elliptical. Hence, for the purpose of numerical analysis, such cracks can be approximated by semi-elliptical profiles. In this Chapter, the effect of the tensile and bending loads on such semi-elliptical cracks in pipe is presented.

4.2 FINITE ELEMENT ANALYSIS OF CRACKED PIPE

4.2.1 Solid model and mesh for analysis

The solid model of the pipe is shown in Fig. 4.1. Figures 4.2 and 4.3 show the $X-Y$ cross section of pipe, in the middle of the length in Z direction. Crack is assumed to have symmetrical shape with respect to the plane 1 and it lies in the "crack plane" (in the middle of the pipe) as shown in Figs. 4.2 and 4.3. Taking the advantage of this symmetry we analyze only half of the pipe. The mesh for the pipe has been generated by a FORTRAN code. One of the meshes generated through the code has been shown in Figs. 4.4 and 4.5. A closer view of the mesh is shown in Fig. 4.6 and the crack-front is shown in Fig. 4.7. The mesh is imported into PATRAN/NASTRAN and elastic analyses are carried out. For the finite element analysis, 8 noded brick (hexahedral) elements have been used.

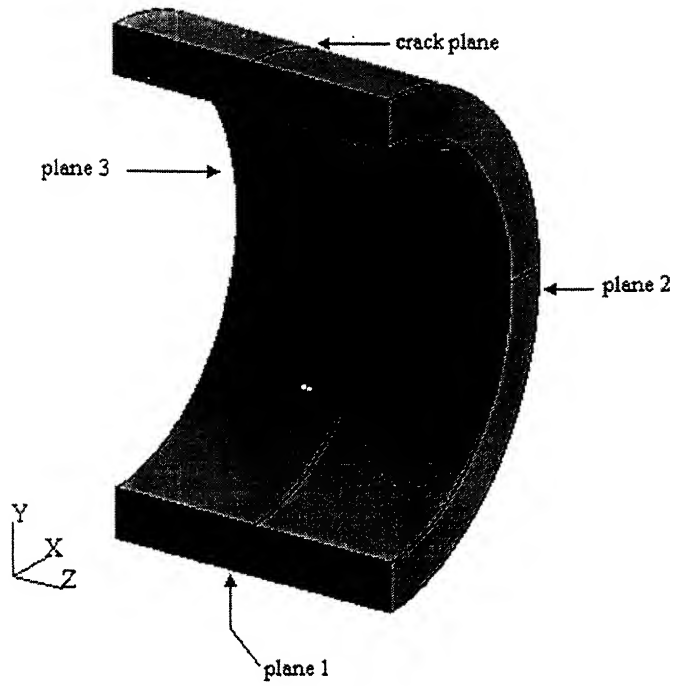

Figure4.1 Isometric view of the solid model of pipe.

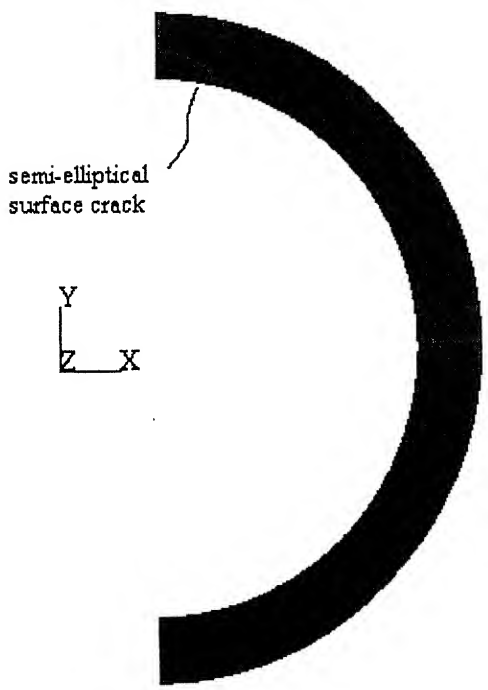

Figure 4.2 Cross-sectional view of pipe with crack.

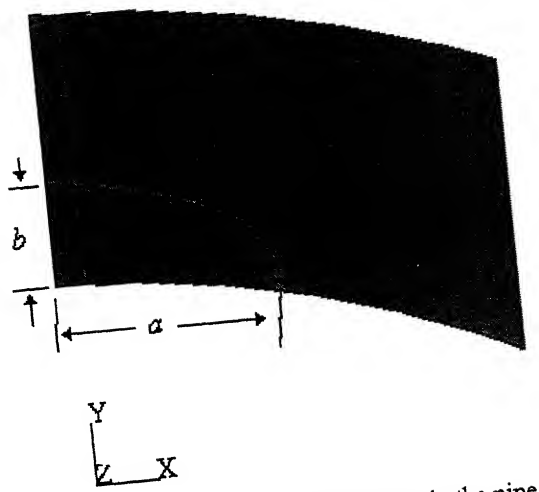

Figure 4.3 Closer view of the crack front in the pipe.

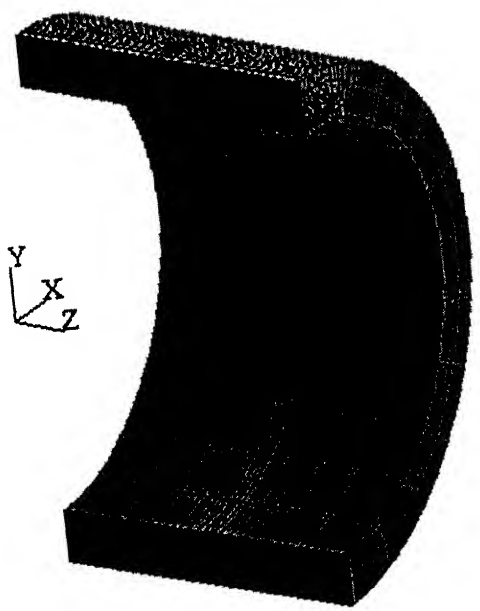

Figure 4.4 Isometric view of a typical mesh.

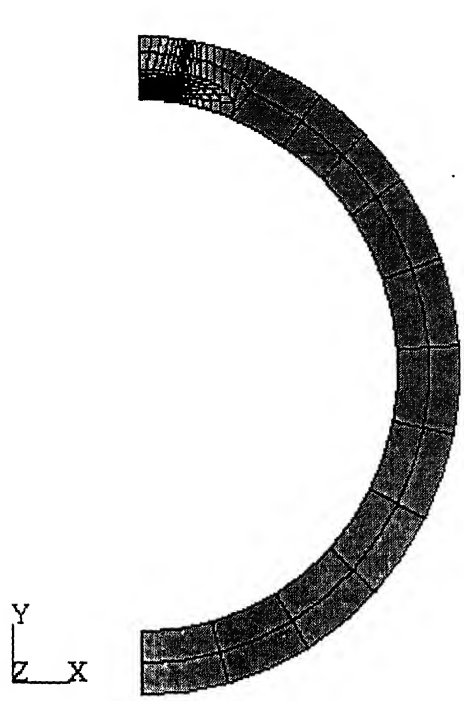

Figure 4.5 Cross-sectional view of a typical mesh.

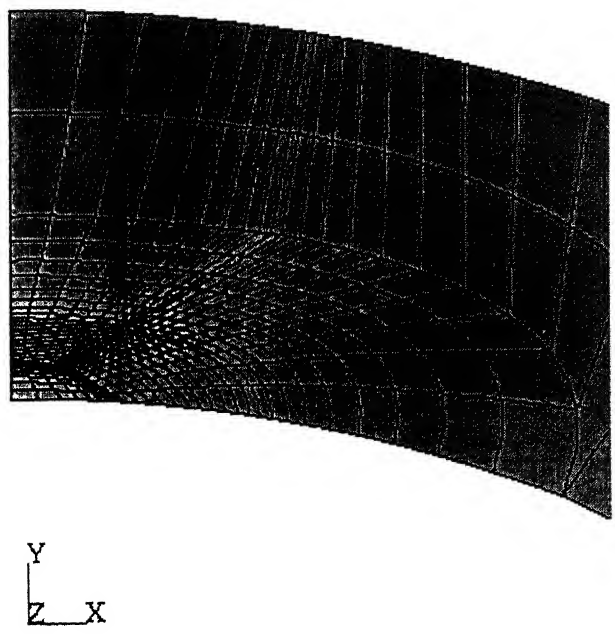

Figure 4.6 Closer view of mesh near crack front.

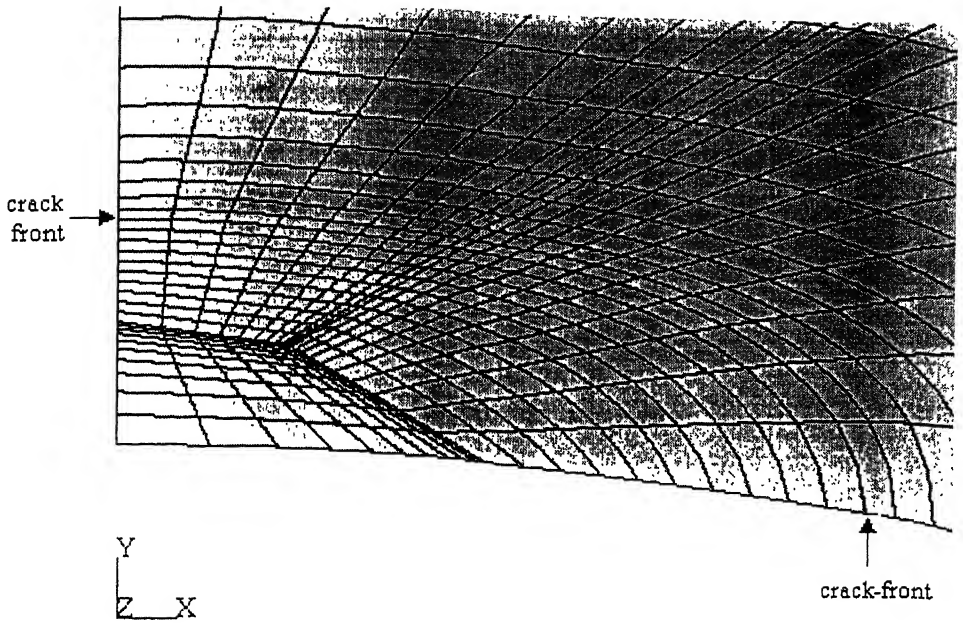

Figure 4.1 Mesh near crack-front.

4.2.1 Geometric and material properties

Geometric data of the pipe provided by BARC Mumbai is as follows:

- Nominal Diameter of the pipe: 267 *mm*
- Thickness of pipe: 32 *mm*

Pipe has a semi-elliptical crack which has semi major axis a and semi minor axis b as shown in Fig 4.3. The semi major axis is along the X direction. A pipe of 50 *mm* diameter is also analyzed for the purpose of determining the effect of pipe diameter on the results. Material data of the pipe for elastic analysis are taken as follows:

- Young modulus: 210 *GPa* and
- Poisson's ratio: 0.30

4.2.2 Loads and Boundary conditions

Since the pressure does not have any effect on opening of the crack, model is analyzed for only two different loadings: tension and bending. The loads are as follows,

Tension: 80 *MPa*

Bending Moment: $25\,kNm$

The problem being elastic, the exact value of the load is not important. Figure 4.1 shows different planes of the solid model on which the load and boundary conditions are applied. As discussed earlier, the model of pipe is symmetric with respect to plane 1. Nodes lying on plane 1 are fixed in the X direction. Plane 3 is fixed in Z direction and the load is applied on plane 2. Rigid body motion in Y direction is restricted by fixing few nodes in the middle part of plane 3.

4.3 RESULTS AND DISCUSSIONS

As stated before, the model is analyzed for two different types of loading: tension and bending. Parametric study is carried out for the two cases. The effect of thickness of weld is also studied.

For the parametric study, the semi major axis a of the elliptical crack is fixed at $20\ mm$ and the value of aspect ratio b/a is varied from 0.3 to 0.8. The J-integral is evaluated over two different domains with 2 and 3 layers of elements around crack front for each case.

4.3.1 Results for tension loading

The results are obtained for tension loading for the semi elliptical cracks of aspect ratio b/a equal to 0.3, 0.4, 0.6 and 0.8 are plotted. The analytical relations for K_I for infinite plate having semi-elliptical edge crack is given by

$$K_I = \frac{1.12\sigma(\pi b)^{1/2}}{I_2}\left[\sin^2\phi + \left(\frac{b}{a}\right)^2\cos^2\phi\right]^{1/4}, \tag{4.1}$$

where,

$$I_2 = \int_0^{\pi/2}\left(1-\frac{a^2-b^2}{a^2}\sin^2\phi\right)^{1/2} d\phi, \tag{4.2}$$

and ϕ is the angle made by the line joining the node on ellipse to the centre of ellipse with X axis[37].

Since the diameter of the pipe ($267\ mm$) is large compared to the crack length (semi major axis a=$20\ mm$), a comparison can be made between the pipe results and the

analytical results for infinite plate. These comparisons are made in the following graphs. Graphs are plotted for the variation of *J*-integral with the angle, where the angle represents the location of crack front node, and it is measured from the centre of the ellipse with respect to *X* axis in counterclockwise direction.

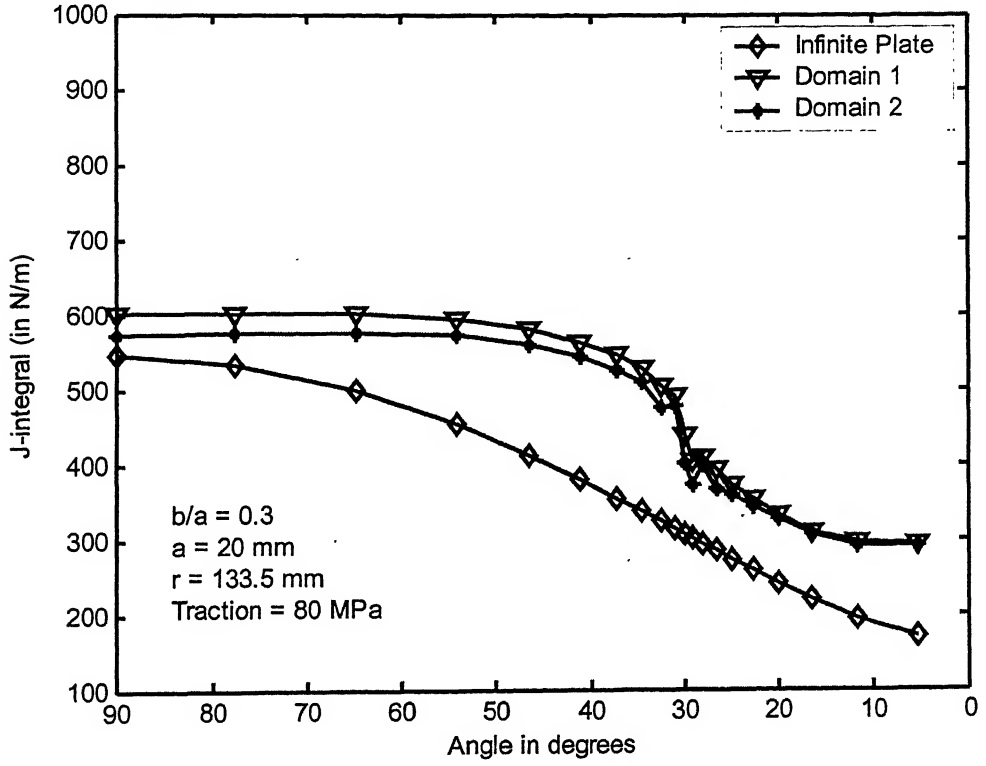

Figure 4.8 Variation of *J*-integral along the crack front for $b/a = 0.3$ and r = 133.5mm in tension

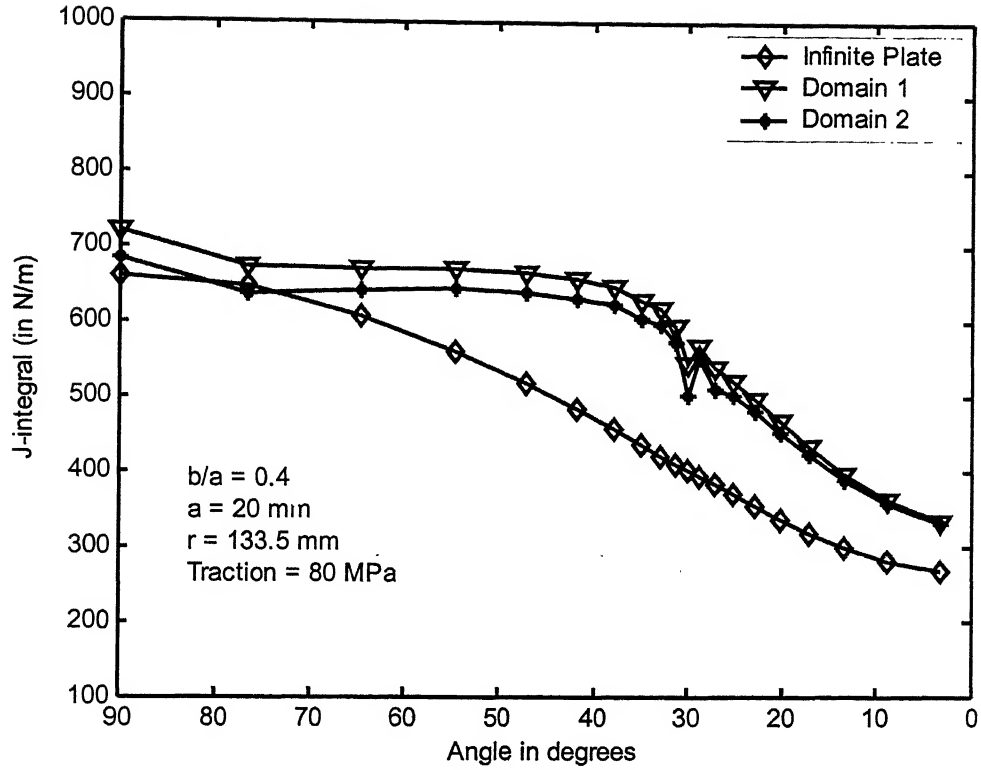

Figure 4.9 Variation of *J*-integral along the crack front for $b/a = 0.4$ and r = 133.5mm in tension

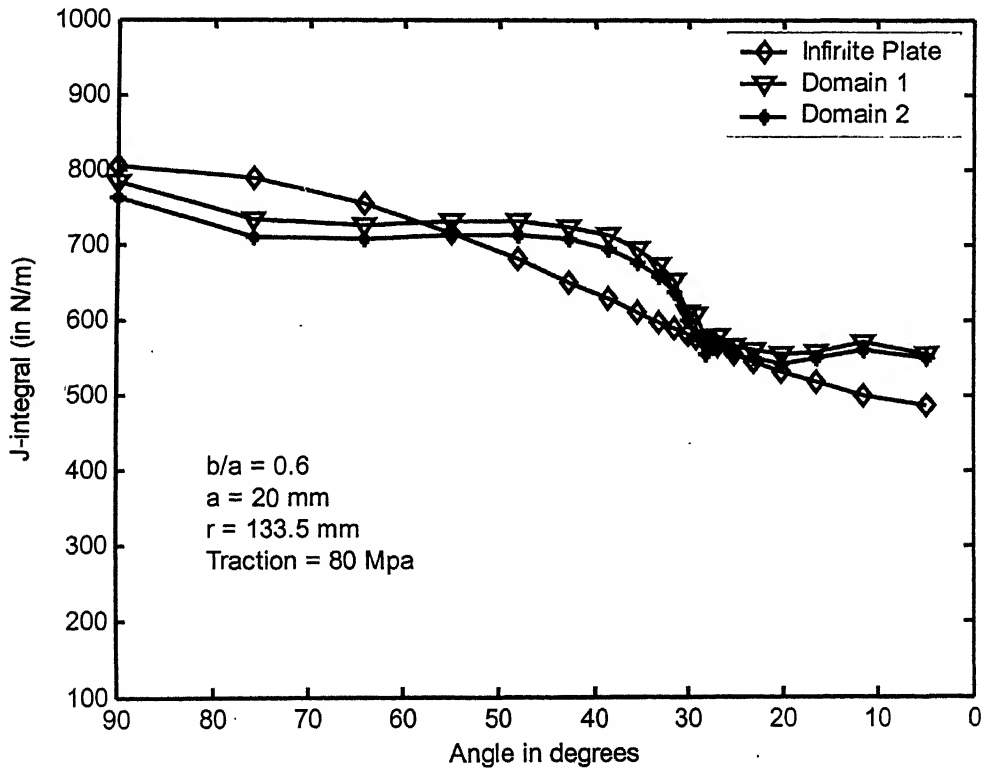

Figure 4.10 Variation of *J*-integral along the crack front for $b/a = 0.6$ and r = 133.5mm in tension.

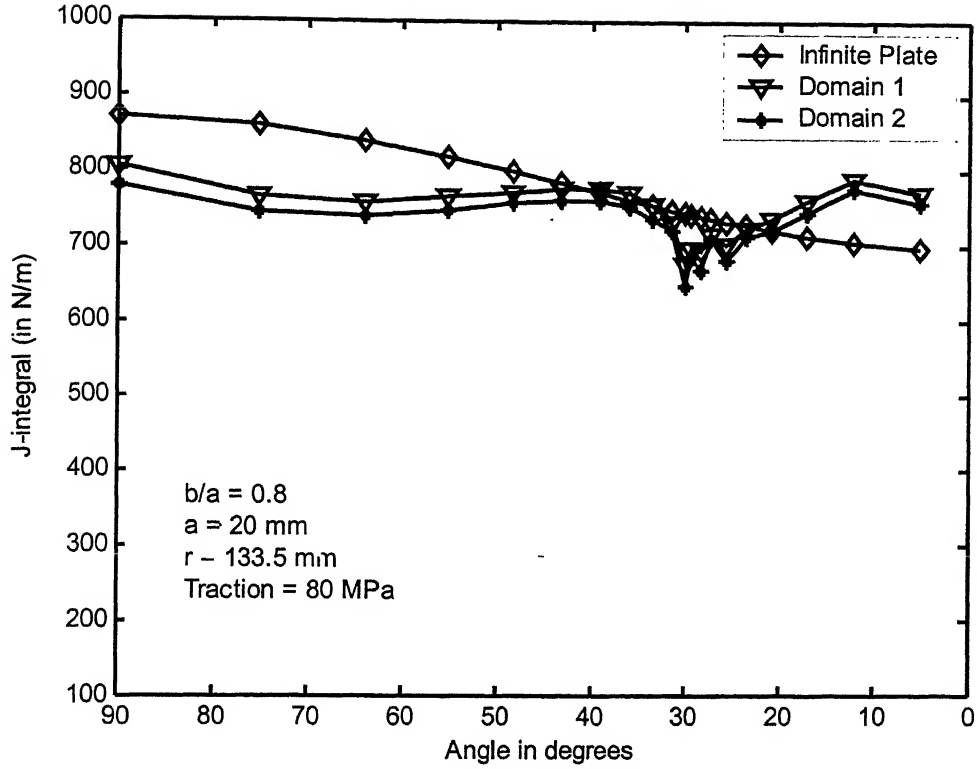

Figure 4.11 Variation of *J*-integral along the crack front for $b/a = 0.8$ and r = 133.5mm in tension

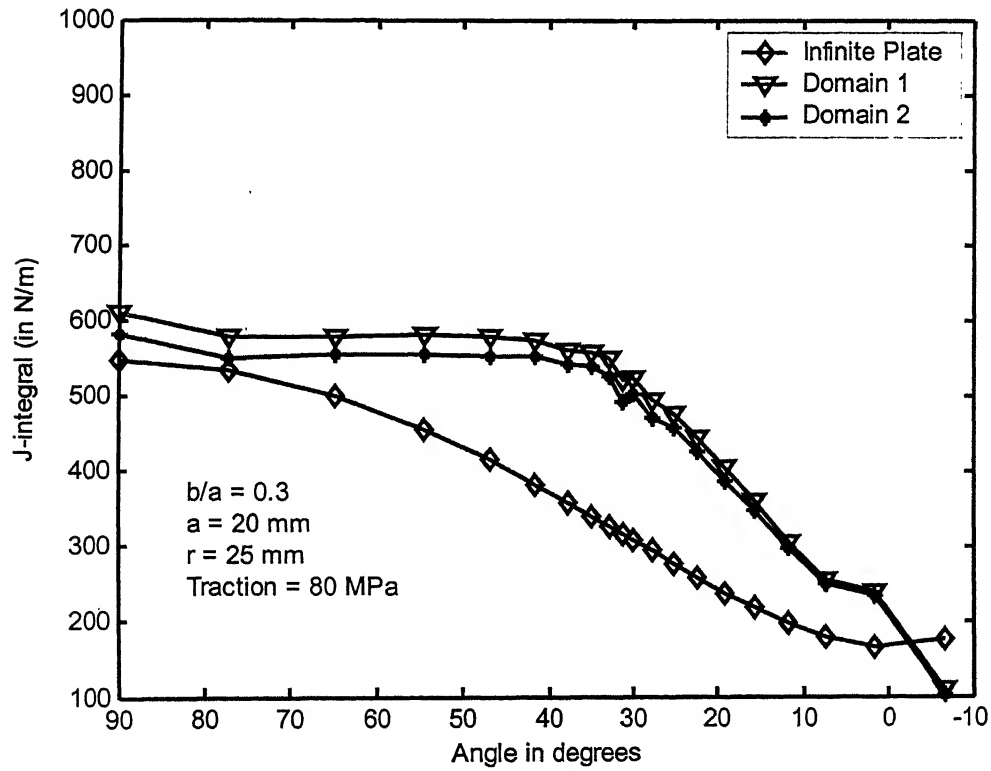

Figure 4.12 Variation of *J*-integral along the crack front for $b/a = 0.3$ and r = 25mm in tension

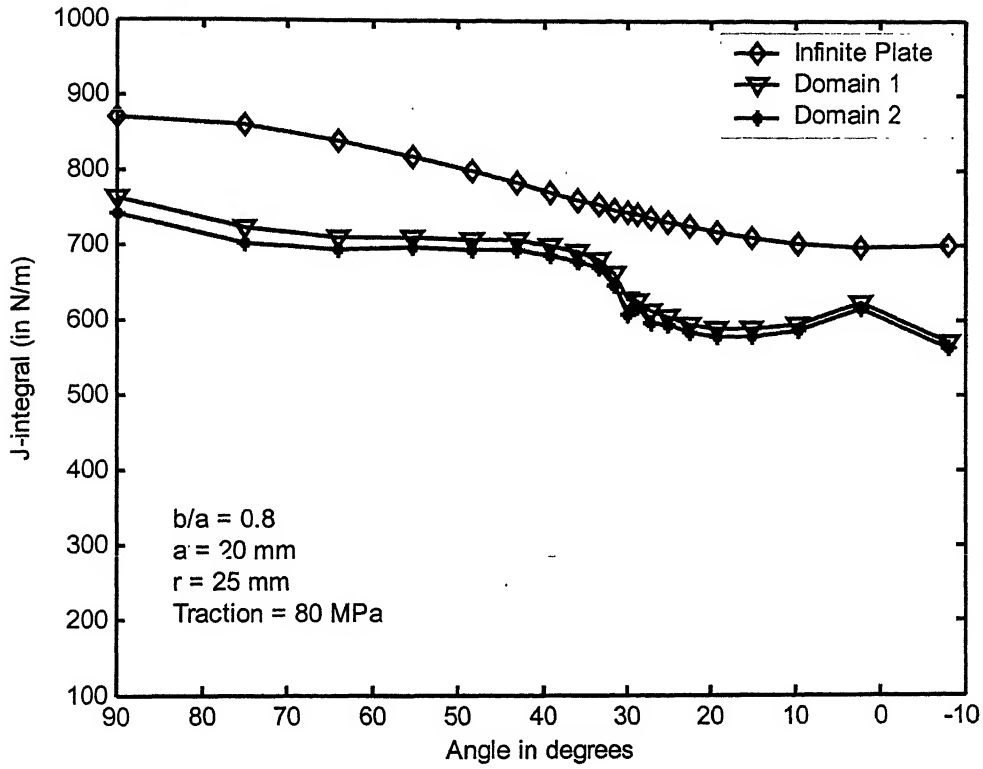

Figure 4.13 Variation of *J*-integral along the crack front for $b/a = 0.8$ and r = 25mm in tension

It is clear from the graphs shown in Figs 4.8 – 4.13 that as the aspect ratio b/a (and hence the crack depth b) increases, value of *J*-integral increases and also the variation of the J-integral along the crack front becomes nearly the same as that for the infinite plate. For b/a ratio less than 0.6, the value of J is maximum at the centre of the crack front (at 90°) and decreases as we move towards the free surface. But for b/a ratio equal to 0.6 or more, the J-integral value is comparable to the maximum value, even at the free surface of the pipe wall. So it can be concluded that for low b/a ratio (less than 0.6), the crack has a tendency to grow in the radial direction which corresponds to the leak-before-break condition. As the b/a ratio increases (more than 0.6), the crack has a tendency of propagating circumferentially which corresponds to the full guillotine offset break (i.e., instantaneous circumferential fracture). So there must be a critical value of the aspect ratio up to which the leak-before-break condition prevails.

Figures 4.12-4.13 are for a pipe of diameter $50\,mm$ for two extreme aspect ratios (b/a = 0.3 and 0.8). From these plots it is clear that radius of pipe have a very little

influence on the value of J-integral. For small b/a ratio, the effect of diameter is negligible, while for larger b/a ratio it is slightly more. So practically, diameter has no effect on the J values when the thickness of the pipe and the aspect ratio b/a remain constant.

4.2.1 Results for bending loading

A similar parametric study is carried out for bending load with the same set of aspect ratios b/a and with the same value of semi major axis ($a=20mm$) . The bending load is applied in a manner that it opens the crack. A bending moment of $25\,kNm$ is applied about X axis on plane 2 in clockwise direction. The results are plotted in the following Figures.

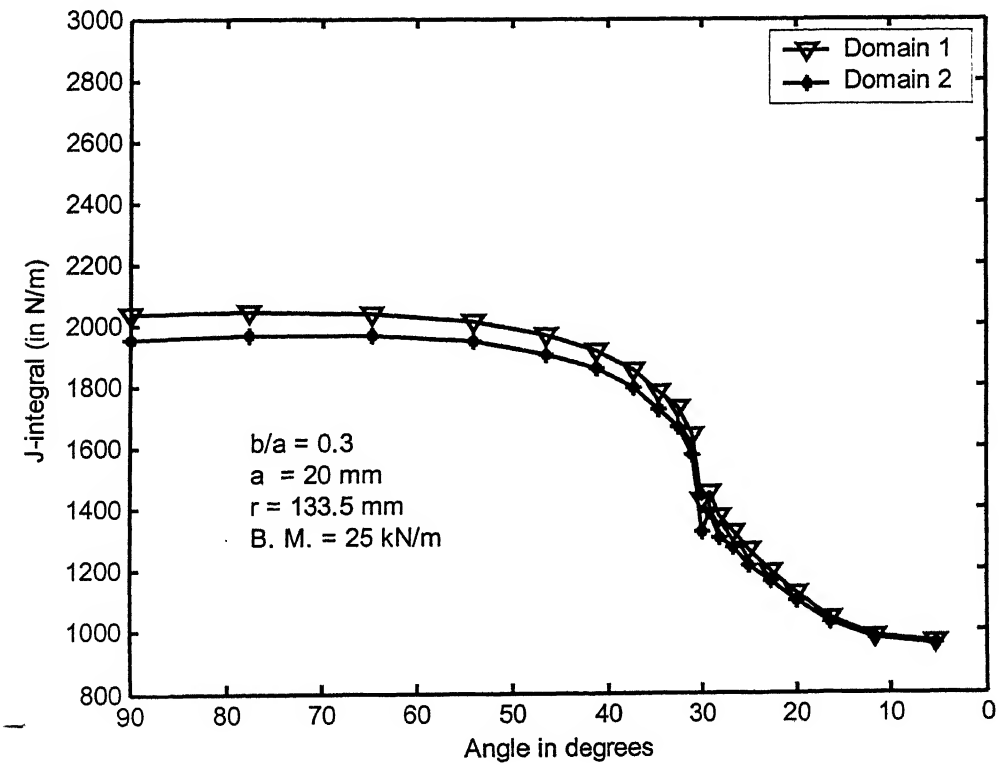

Figure 4.16 Variation of J-integral along the crack front for $b/a = 0.3$ and r = 133.5mm in bending.

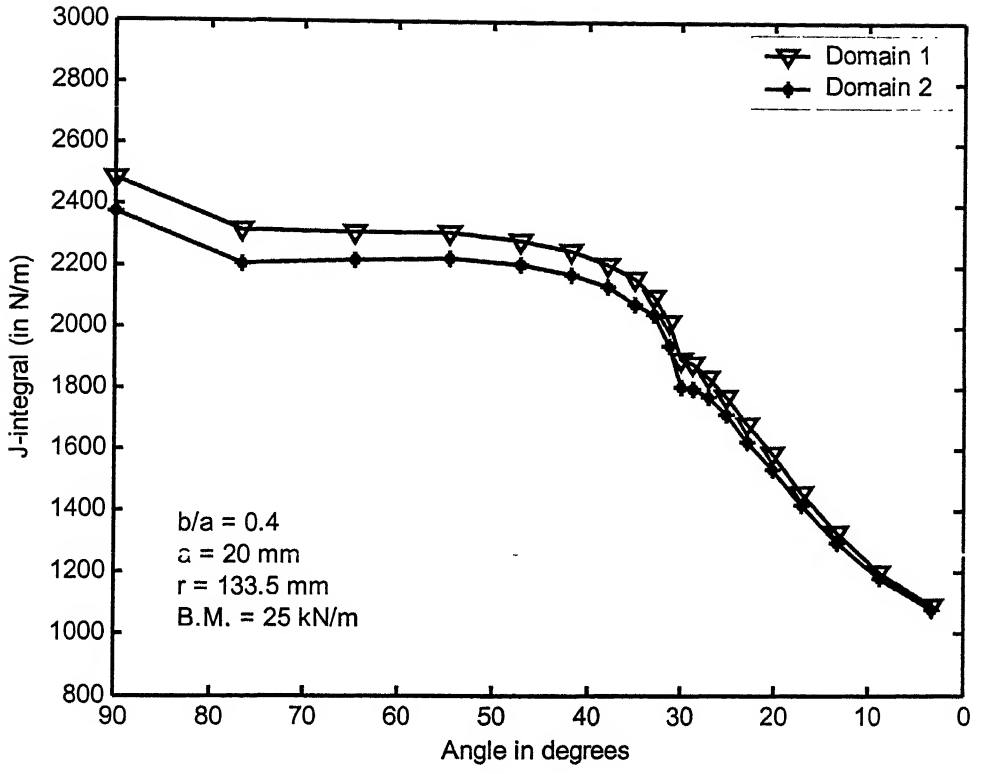

Figure 4.15 Variation of *J*-integral along the crack front for $b/a = 0.4$ and r = 133.5mm in bending.

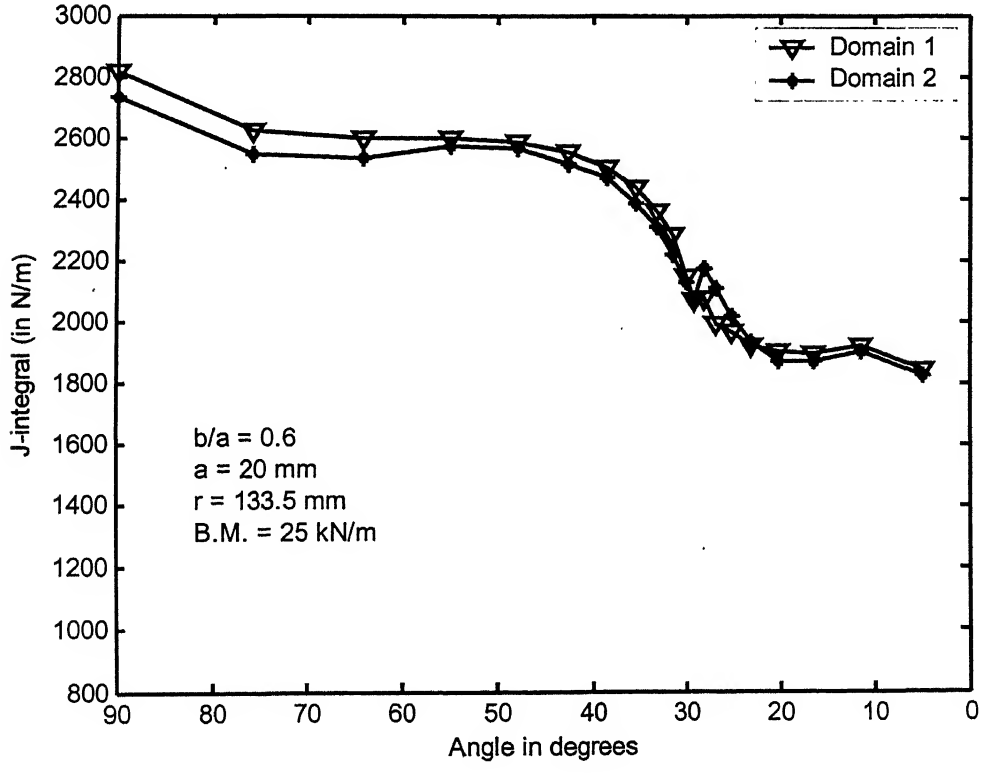

Figure 4.16 Variation of *J*-integral along the crack front for $b/a = 0.6$ and r = 133.5mm in bending.

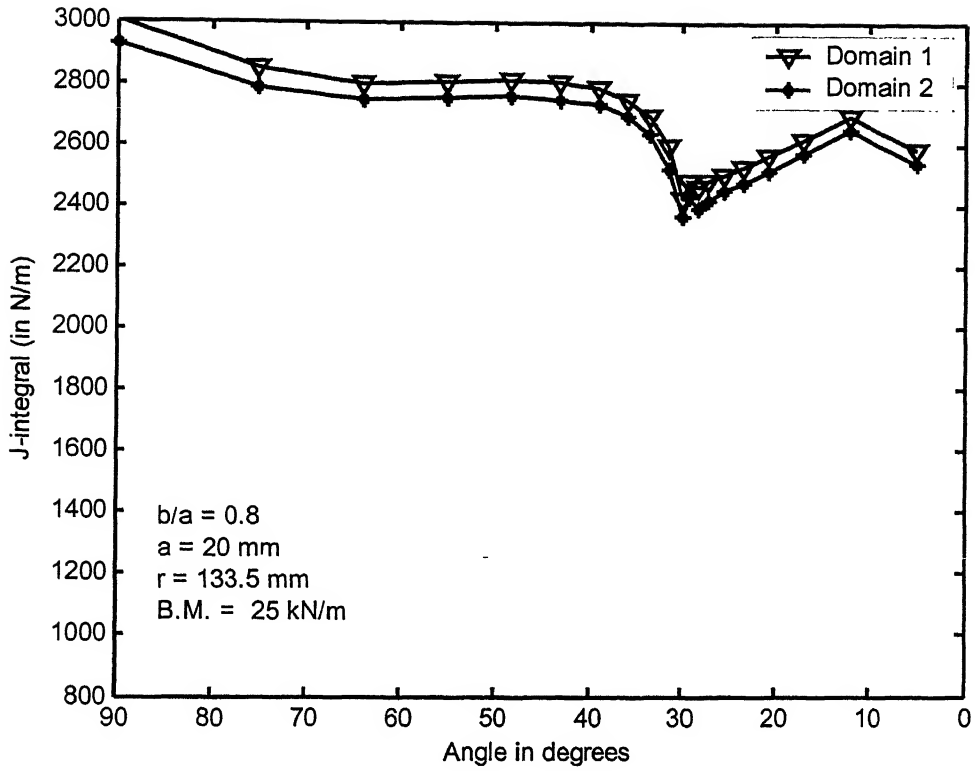

Figure 4.17 Variation of *J*-integral along the crack front for $b/a = 0.8$ and r = 133.5mm in bending

It is clear from Figs. 4.14-4.17 that the trend is same as in case of tension and it is expected because the state of stress created by bending moment near the crack is same as that in tension. As the aspect ratio b/a increases, the *J*-integral increases and the curve gets flatted (same as in the case of tension).

CHAPTER 5
CONCLUSIONS AND SCOPE FOR FUTURE WORK

5.1 CONCLUSIONS

In the present work a Matlab code has been developed to evaluate the 2-D *J*-integral. The results obtained for SENB, CT and CP specimen in plane strain condition have shown good agreement with analytical solutions.

The 2-D code has been extended to evaluate the point-wise *J*-integral along the curved crack front for the 3-D crack problems. The values of *J*-integral of the 3-D crack problems have also been successfully validated with the analytical results pertaining to plane strain problems.

Variation of point-wise *J*-integral along the crack front in a cracked pipe having a semi elliptical crack has been obtained and parametric study has been carried out by varying the aspect ratio and keeping the pipe geometry and semi major axis of the elliptical crack fixed. These parametric analyses have been carried out for two different types of loadings namely bending and tension. The trend obtained for tension case has also been compared successfully with for an infinite plate with semi elliptical edge crack in tension. The results obtained from bending analysis are having the same trend as in case of tension.

5.2 SCOPE FOR FUTURE WORK

The desired future extensions of this work have been listed below:

1. Currently the program uses elastic stress and strain to evaluate the *J*-integral. The program can be extended to evaluate *J*-integral for elasto-plastic large deformation problems by incorporating appropriate constitutive theories.

2. The effect of thermal strains can be included by introducing thermal strain terms in the *J*-integral expression.
3. The *J*-integral for dynamic problems can also be evaluated by adding appropriate dynamic terms in the *J*-integral expression.

REFERENCES

1. J. R. Rice, Mathematical analysis in the mechanics of fracture, in *Fracture: An Advanced Treatise* (Edited by H. Liebowitz), Vol.2, pp.191-311. Academic Press, New York (1968).
2. J. R. Rice, A path independence integral and the approximate analysis of strain concentration by notches and cracks. *J. appl. Mech.* **35,** 379-386 (1968).
3. G. P. Chereponov, crack propagation in continuous media. J. app. Math. Mech. (translation of PMM) **31,** 476-488 (1947).
4. J. D. Eshelby, The continuum theory of lattice defects, in Progress in solid state Physics (Edited by F. Seitz and D. Turnbull), Vol. 3, pp. 79-144. Academic Press New York (1956).
5. J. D. Eshelby, Energy relations and the energy momentum tensor in continuum mechanics, in *Inelastic Behaviors of Solids* (Edited by M. F. Kanninen *et al.*), pp. 77-114. McGraw-Hill, New York (1970).
6. J. K. Knowles and E. Sternberg, On a class of conservation laws in linearized and elatostatics. *Arch. ration Mech. Anal.* **44,** 187-211 (1972).
7. B. Budiansky and J. R. Rice, Conservation Law and energy release rates. *J. appl. Mech.* **40,** 201-203 (1973).
8. J. W. Hutchinson, Singular behavior at the end of a tensile crack in a hardening material. *J. Mech. Phys. Solids* **16,** 13-31 (1968).
9. J. R. Rice and G. F. Rosengren, Plain strain deformation near crack tip in a power law hardening material. *J. Mech. Phys. Solids* **16,** 1-12 (1968).
10. K. Kishimoto, S. Aoki and M. Sakata Dynamic stress intensity factors using $\hat{J}$-integral and finite element method. *Engng. Fracture Mech.* **20,** 387-394 (1982).

23. D. M. Parks, A stiffness derivative finite element techniques for determination of crack tip intensity factors. *Int. J Fracture* **10,** 487-502 (1974).

24. D. M. Parks, The virtual crack extension method for nonlinear material behavior. *Comp. Meth. Appl. Mech. Engng* **12,** 353-364 (1977).

25. T. K. Hellen, On the methods of virtual crack extension. *Int. J. numer. Meth. Engng.* **9,** 187-207 (1975).

26. H. G. deLorenzi, On the energy release rate and *J*-integral for 3-D crack configuration. *Int. J. Fracture* **19,** 183-193 (1982).

27. B. Moran and C. F. Shih, Crack tip and associated domain integrals from momentum and energy balance. *Engng. Fracture Mech.* **27,** pp. 615-642 (1987).

28. C. Atkinson and J. D. Eshelby, *International Journal of Fracture Mechanics* **4** 3-8 (1968).

29. B. V. Kostrov and L. V. Nikitin, *Archiwum Mechaniki Stosowanej* **22** 749-775 (1970).

30. L. B. Freund, *Journal of Elasticity* **2** 341-349 (1972).

31. T. Nakamura, C. F. Shih and L. B. Fruend, *International Journal of Fracture* **27** 229-243 (1985).

32. O. C. Zienkiewicz, *The Finite Element Method,* McGraw-Hill, London, England (1977)

33. A. Bakker, An analysis of the numerical path dependence of *J*-integral, Int. J. Pres. Ves. & Piping **14** (1983) 153-179.

34. Annual Book of ASTM Standards. Metals test methods and analytical procedures, ASTM Publications, Philadelphia, 03.01, 552-557 (1987).

35. E. E. Gdoutos, *Fracture Mechanics-An Introduction*, Kluwer Academic publishers, Dordrencht (1993).

36. H. G. deLorenzi and C. D. Shih, 3-D Elastic-plastic investigation of fracture parameters in the side grooved compact specimen, *Int. J. of fracture*, **21**, 195-220 (1983).

37. P. Kumar, *Elements of Fracture Mechanics*, Wheeler Publishing, New Delhi, (1999)